UNDERSTANDING EXCITON DIFFUSION IN ORGANIC SOLAR CELLS

Amy Illingworth

A Thesis Submitted for the Degree of MPhil
at the
University of St Andrews

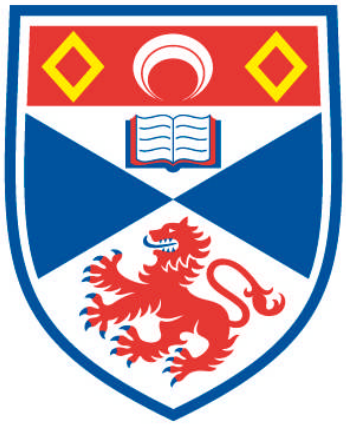

2012

Understanding Exciton Diffusion in Organic Solar Cells

MPhil

Amy Illingworth

Organic solar cells are promising candidates for future energy production. However, many challenges remain to optimise efficiency. One particular challenge lies in our understanding of the factors affecting exciton diffusion and the length scale of this process. This is particularly relevant to morphology optimisation for organic solar cells. A powerful tool to gain insight into this is femtosecond photophysical measurements.

This thesis details work undertaken at the University of St Andrews between September 2009 and December 2010 towards a Masters of Philosophy. It includes an introduction to the field and a description of experimental methods used. Experimental chapters discuss measuring the optical constants of P3HT, a study of low concentration volume quenching, surface quenching measurements using titanium dioxide, surface quenching measurements using other quenchers and an investigation of the thickness dependence of the photoluminescence decay time in thin polymer films.

Declaration

I, Amy Illingworth, hereby certify that this thesis, which is approximately 16,500 words in length, has been written by me, that it is the record of work carried out by me and that it has not been submitted in any previous application for a higher degree.

I was admitted as a research student in September 2009 and as a candidate for the degree of MPhil in November 2011; the higher study for which this is a record was carried out in the University of St Andrews between 2009 and 2010.

Date Signature of candidate

I hereby certify that the candidate has fulfilled the conditions of the Resolution and Regulations appropriate for the degree of MPhil in the University of St Andrews and that the candidate is qualified to submit this thesis in application for that degree.

Date Signature of supervisor

Declaration of Copyright

Chapter 1

Introduction to the Field

1.1 Motivation for Research into Organic Solar Cells

Our global economy and standard of life depend on the availability of cheap, reliable energy. As the population grows, the pressure on energy resources is increasing. Traditional energy sources such as coal, oil and gas will no longer meet our energy needs and are environmentally unsustainable. A stable, effective energy policy must include a broad range of energy sources. Renewable energy is required.

Many scientists believe that solar power is a vital untapped source of energy[1].The Sun provides the Earth with 8×10^{21} Joules each day, equivalent to 200 million coal power stations[2]. This vast source of energy can be exploited in the form of passive solar heating systems or photovoltaics. Whilst passive solar heating has had some uptake, photovoltaics are rarely used. In 2006 the worldwide percentage of energy generated by solar thermal was 0.5%, whereas photovoltaics accounted for 0.04%[3]. This is largely due to the expense of photovoltaic systems. Inorganic semiconductor solar cells can achieve laboratory power conversion efficiencies in excess of 40%[4], but use expensive processing to ensure semiconductor purity. The amorphous silicon solar cells commercially available have efficiencies of 12-15%. Other options such as cadmium indium gallium selenide solar cells are available, yet issues still remain with price and efficiency.

Solar cells made from organic semiconductors present an alternative. Due to the solubility of organic semiconductors low cost processing methods such as roll to roll printing are envisaged. There are some sceptics of the potential of organic solar cells, however recent research interest has led to an increase in power conversion efficiencies from 0.1 % in the early 90's to 8.13% this year[5]. Further research and improvements in efficiency are required before commercialisation can occur.

One driving factor behind the research is the recent commercialisation of another organic semiconductor technology. It is now possible to buy mobile phones and televisions with organic light-emitting diode displays. Many current OLED displays follow from the work of Tang and Van Slyke at Kodak[6].

1.2 Organic Semiconductors

1.2.1 Chemistry of Organic Semiconductors

To understand the properties of organic semiconductors a basic knowledge of their chemical structure is required. Most materials based around carbon are considered to be organic materials.

1.2.2 The Chemistry of Carbon

Carbon's atomic configuration is $1s^2 2s^2 2p^2$. The p orbital has three parts, orientated in different directions, known as p_x, p_y and p_z. The outermost electrons are the $2p^2$ electrons, which lie in the p_x and p_y orbitals. These are unpaired and should form two bonds, to allow the electrons to pair. However, by a process known as promotion and hybridisation, the $2s^2$ electrons are joined with the $2p^2$ electrons to allow four bonds to form.

The simplest arrangement is for one of the $2s^2$ electrons to be promoted to the empty p_z orbital. The three p orbitals and the remaining s orbital then hybridise, to create the sp^3 orbital. This orbital has four unpaired electrons, lying at an energy level between the 2s orbital and the 2p orbital. The electrons are equally spaced in three dimensions, and when paired in bonds form the classic tetrahedron structure seen in molecules such as methane.

Other hybridisations are possible. The most important arrangements for conjugated molecules are sp^2 and sp. The sp^2 arrangement has three hybridised electrons and one remaining in the p_z orbital. The sp^2 electrons lie together in the x-y plane, with the p_z orbital perpendicular to them in the z plane.

The sp arrangement has two hybridised electrons in the sp orbital and an electron in p_y and p_z. The sp orbital electrons lie in the x plane, and the two p orbital electrons are in the y and z plane.

1.2.2 Molecules built from Carbon

In the sp^2 configuration, the three sp^2 hybrid electrons can form single bonds within their plane. These are known as σ bonds. The remaining p_z electron forms a delocalised bond, in the z plane around the σ bonds. This is known as a π bond, and the combination of a σ bond and a π bond is known as a double bond. This is sometimes referred to as conjugation, with molecules containing double bonds known as conjugated molecules.

Considering several carbon atoms, conjugation can occur when single and double bonds connect a chain of carbon atoms. This is known as known as linear conjugation. Due to the delocalised nature of the π bond, it is possible for the π bond to move along the chain of bonded carbon atoms. This allows the conduction of electricity to occur in systems containing carbon atoms joined by alternating single and double bonds.

Different carbon atoms can also join together in planar systems. An example of this is a benzene ring, as shown in Figure 1. Six carbon atoms are arranged in a hexagon. Six σ bonds maintain the hexagonal structure. Three π bonds are delocalised above and below the plane, creating a ring of delocalised electrons. Benzene rings are the building blocks of many conjugated systems.

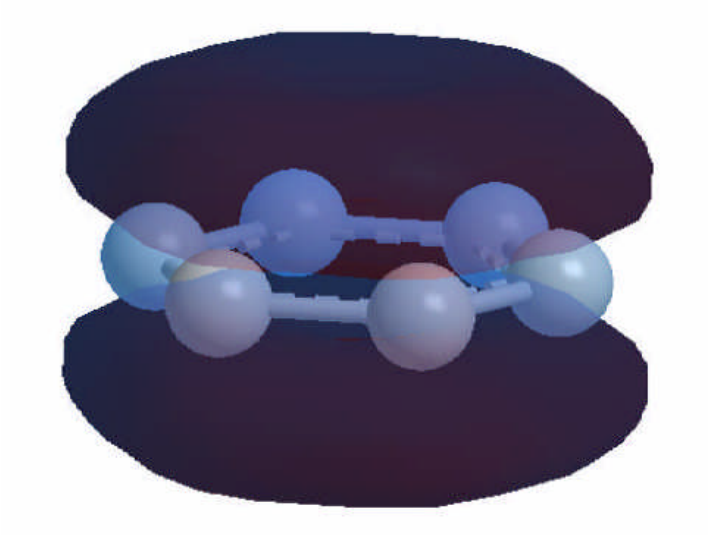

Figure 1. A benzene ring. The delocalised π bond can be seen above and below the ring of carbon atoms. The sigma bonds are represented by cylinders.

1.2.3 Photogenerated Excitations

In a π bond the orbitals overlap in phase and constructively interfere. It is also possible for the orbitals to overlap out of phase and destructively interfere. This occurs at a slightly higher energy cost and is known as a π* bond.

Due to the higher energy cost, the π* state can be excited by absorption of a photon. When this occurs, an electron moves from the highest occupied molecular orbital (HOMO) to the lowest unoccupied molecular orbital (LUMO). The gap between these two orbitals is analogous to the band gap in inorganic semiconductors. In large conjugated systems, the π electrons will be spread out over a large distance, leading to a reduction in energy[7]. This means that optical transitions are in the visible region for large conjugated systems.

When an electron moves from the HOMO to the LUMO and the molecule enters a π* anti-bonding state a re-arrangement of the nuclei occurs. This is because there is reduced electron density between the nuclei, so increased repulsion, forcing the nuclei further apart. This re-arrangement is the origin of the higher energy cost of anti-bonding orbitals. This is shown in Figure 2a, where the excited state is displaced from the ground state, due to the greater distance between the nuclei (R).

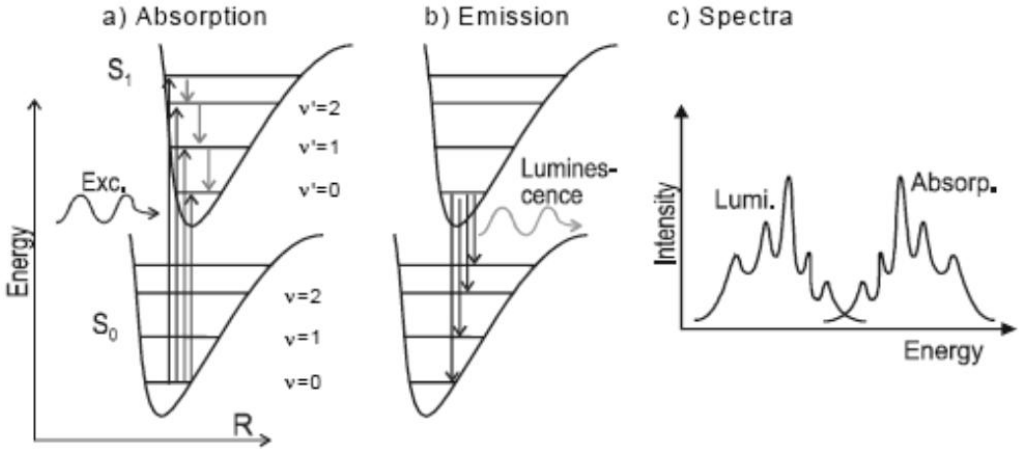

Figure 2. A representation of the energy levels in an organic material. a) arrows show absorbed light b) arrows show emitted light c) the idealised absorption and emission spectra are mirror images. Figure from reference 7.

The potential energy of the nuclei's displacement can be considered as a harmonic oscillator, with quantised energy levels of spacing ħω. In Figure 2a, the quantised energy levels in both the ground state and the excited state are shown. The spacing of the quantum levels is the same in both states, as the harmonic oscillator has only been displaced by the nuclear separation, not altered. Transitions can occur between these quantum levels.

The electrons in the ground state are in the lowest quantum level (v=0).When a high energy photon is absorbed, providing energy for movement to the excited state, the electrons can move to any of the quantum levels available in the excited state. In an ideal quantum system, this means there is a series of discrete absorption peaks in the absorption spectrum as these are the photon energies which match the energy difference between the quantum levels (Figure 2c).

Once in the excited state, the electrons relax to the lowest quantum level by phonon interactions. From this position, the electrons can relax back to the ground state. It is possible for the electron to return to any of the quantum levels in the ground state. Due to the change in energy when relaxing back to the ground state, a photon is released. This is known as luminescence. The released photon will have an energy equivalent to the energy gap between the lowest quantum level of the excited state and the quantum level in the ground state which it moves to. As there are several quantum levels in the ground state, there are several possible energies at which photons can be emitted. This gives rise to discrete peaks in the emission spectrum. The pattern of the peaks in the emission spectrum is a mirror image of the peaks in the absorption spectrum, as the harmonic oscillators in both states are equivalent.

It is also possible for relaxation from the excited state to the ground state to occur without the emission of a photon. The energy lost on relaxation is distributed through phonon interactions. This is a problem in organic LEDs, as less photons are emitted from the OLED.

1.2.4 Excitons

The movement of an electron to the LUMO creates a hole in the HOMO. The electron and hole are attracted together by the Coulomb force, and bind to create a particle known as an exciton. In organic semiconductors, due to small dielectric constants, excitons are tightly bound and localised to the individual molecule. This type of exciton is properly referred to as a Frenkel exciton to differentiate it from the free electrons found in inorganic systems. Throughout this work the term exciton will be used to refer to the bound excitons found in conjugated systems.

The exciton binding energy is 0.5 eV, roughly an order of magnitude greater than kT[8], so excitons are stable at room temperature. Excitons can travel through the semiconductor, by delocalisation along the molecule or by hopping from molecule to molecule. The hopping process occurs by Förster transfer (discussed in Section 1.5), a short range dipole-dipole transfer mechanism with a length scale of around 5 nm. This process moves the exciton gradually to molecules with lower energy states, where it becomes localised. The exciton can also hop between conjugated segments of a polymer chain. The average distance travelled by an exciton during its lifetime is known as the exciton diffusion length, which is given the symbol L_D.

1.2.5 Singlet and Triplet Excitons

Due to the spin alignment of electrons, it is possible for excitons to have spin 0 or spin 1. There are three possible configurations in which the excitons can have spin 1, but only one for spin zero. The spin states are therefore known as triplets and singlets respectively. The ground to spin 0 state is the transition which occurs when light is absorbed, so singlet excitons are the most important for solar cells. Triplets lie at lower energy than singlets. The ground to spin 1 transition is forbidden due to spin conservation rules. Triplets can only be formed by relaxation from the singlet state in a weakly allowed process called inter-system crossing. Triplets are of importance in organic LEDs.

1.3 Organic Solar Cells and their Operation

1.3.1 The Operation of an Organic Solar Cell

For a solar cell to operate light must be absorbed to create excitons. The excitons must then be split into electrons and holes to allow charge transport to the electrodes. Charge extraction then occurs from the electrodes.

Exciton splitting is commonly achieved by using a donor molecule which absorbs incident light and an acceptor molecule which takes electrons and conducts them to the cathode. Exciton splitting only occurs at the interface between a donor and acceptor, so excitons must diffuse through the donor to reach an interface with the acceptor. The most commonly used materials are Poly(3 hexyl)thiophene (P3HT) as the donor and Phenyl-C61-butyric acid methyl ester (PCBM) as the acceptor, which are capable of achieving power conversion efficiencies of 5% in a blend[9]. Their molecular structures are shown in Figure 3.

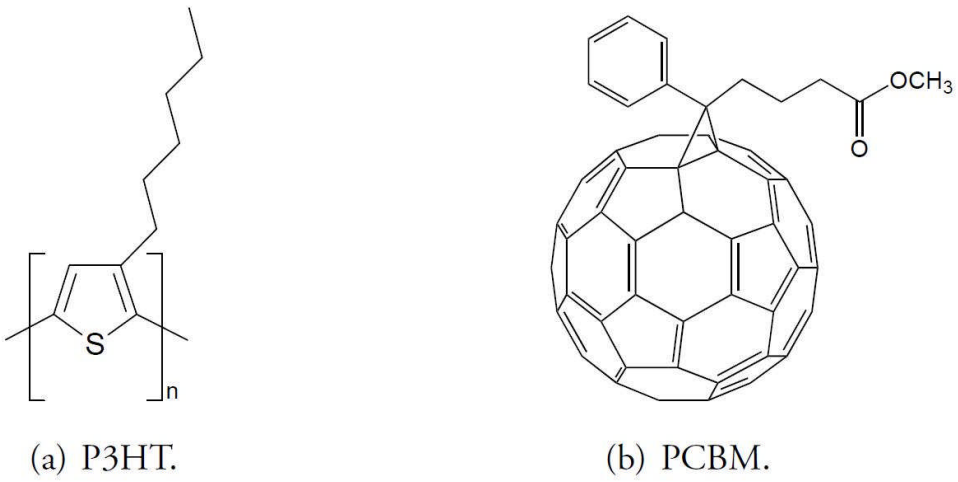

(a) P3HT. (b) PCBM.

Figure 3. The molecular structures of P3HT (a) and PCBM (b)

P3HT is a conjugated polymer with peak absorption at 550 nm. This is in line with the solar spectrum, and gives P3HT a deep red colour. The thiophene rings which from the conjugated backbone mean that P3HT is good hole conductor.

PCBM is a functionalised fullerene molecule. The fullerene can accept up to six electrons, so is an excellent acceptor. The fullerene has an ester chain added to improve solubility. There are several different sizes of fullerene available, with C_{60} the most commonly used.

The HOMOs and LUMOs of P3HT and PCBM align such that excitons can easily be split (Figure 4). The energy difference between the P3HT and PCBM is greater than the binding energy of the exciton. Once an exciton has reached a donor/acceptor interface it can be split. The electron can move from the LUMO of the P3HT to the LUMO of the PCBM. This leaves the hole on the P3HT. The electron can them move through the PCBM to another material with a suitable energy level, such as aluminium. The hole can move through the P3HT to a material with a suitable level for accepting the hole, such as ITO. This process of light absorption followed by exciton diffusion, exciton splitting and charge transport to electrodes is the basic operation of an organic solar cell.

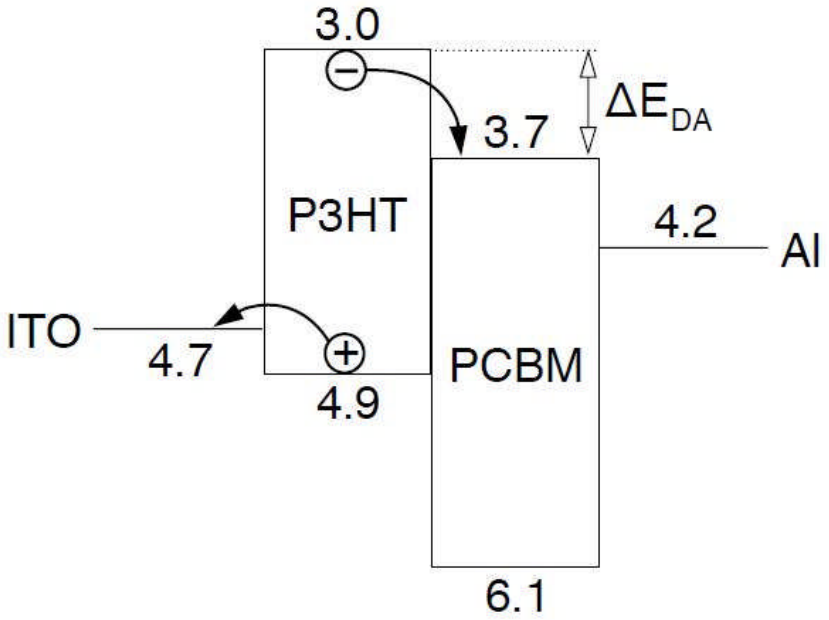

Figure 4. The Energy Levels of a P3HT/PCBM Solar Cell with ITO and Aluminium Electrodes[18].

1.3.2 Structure of Organic Solar Cells

The structure of a bilayer organic solar cell is represented in Figure 5 below. It represents all the stages in the operation of an organic solar cell. The large black arrow shows a photon passing through the transparent ITO to be absorbed in the donor polymer. This creates an exciton, which then diffuses through the polymer to reach the donor/acceptor interface. Here the exciton is split, to create a hole in the donor and an electron in the acceptor. The charges then move to their respective electrodes. At each stage in this process limiting factors occur.

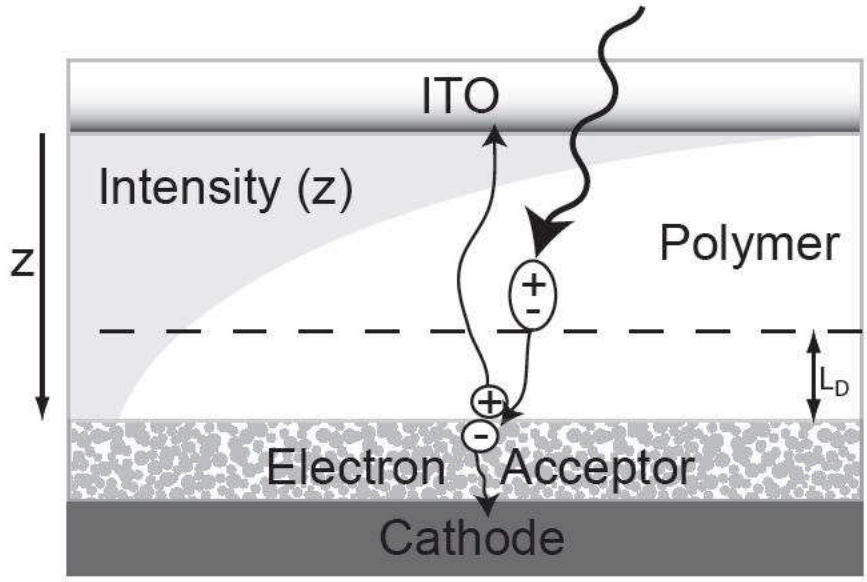

Figure 5. The structure of a bilayer organic solar cell. The process of light absorption, exciton diffusion, exciton splitting and charge transport is shown. The exciton diffusion length is represented, as excitons outwith this region will not reach the donor/acceptor interface. The intensity of incident light is also shown[19].

1.3.3 Limiting Factors for Organic Solar Cells

The absorption of light is limited by the spectral overlap between the absorbing material and the solar spectrum[10]. The majority of semiconducting polymers have a high bandgap, so are able to absorb much of the solar spectrum. However, the low energy infrared radiation which forms a small but significant part of the solar spectrum is missed. Improvement is possible with the development of lower bandgap materials. The amount of absorbing material is also a factor, a layer of 300 nm is generally sufficient to absorb the majority of incident sunlight[11].

The movement of excitons is considered to occur by a combination of exciton delocation along polymer chains, and self Förster transfer. The length scale of this diffusion process depends upon the material, 8.5 nm has been reported for P3HT[12]. Evidently the optimum absorption length is much greater than the exciton diffusion length. This is a major hold back in the operation of bilayer solar cells. In bilayer devices many excitons are formed too far from the donor/acceptor layer and dissociate before they can be split into useful charge. In bilayer devices there is a direct link between exciton diffusion and device performance.

This dilemma is often bypassed by intimately mixing the donor and acceptor, which is known as a bulk heterojunction device. The ideal mixture balances the competing factors of the largest possible donor acceptor interface, and the shortest possible pathways for charge transport. This balance is possible by controlling the phase separation by choice of solvent and annealing conditions. The challenges in achieving optimum morphology reduce the performance of bulk heterojunction devices.

Charge transport is also a limiting factor in organic solar cells, as most organics have inherently poor charge transport properties. For example, P3HT has a hole mobility of 3×10^{-4} cm^2/Vs and an electron mobility of 1.5×10^{-4} cm^2/Vs[13]. Again a small distance is favoured for charge transport, contrasting with the large distances required for optimum absorption.

Another possibility for device improvement lies with the optical interference caused by metallic electrodes. By careful selection of layer thicknesses it is possible to

ensure that the optical interference peaks lie within the active layer, ensuring maximum absorption.[14,15]

As can be seen from the contradiction between the optimum conditions for absorption (thick organic layers) and exciton diffusion (thin organic layers); there is a strong relationship between many of the factors leading to the best device performance. It is possible to optimize for one factor whilst reducing the efficiency of another. Device optimization to date has largely occurred via a process of trial and error[16] due to a lack of understanding regarding many of the individual factors. Understanding of the exciton diffusion length is particularly important in this context. Greater knowledge could lead to materials with longer diffusion lengths and to improved methods for finding the optimum morphology for bulk heterojunctions.

1.3.4 Morphology

Morphology in organic solar cells is determined by the phase separation of the donor material and the acceptor material. Phase separation is very common in polymer systems as for a molecule of N monomer units, the energy of mixing is N times greater than for a single monomer. Therefore only a small unfavourable interaction between polymers can be tolerated before phase separation occurs[17]. Phase separation is used to great advantage in bulk heterojunction solar cells, as it allows a balance between charge separation and charge extraction.

A perfect mixture of materials would lead to the largest possible donor acceptor interface, and allow the maximum number of excitons to reach these interfaces. However, once separated the charges would be confined to individual molecules and unable to contribute to photocurrent. To enable charge transport undisturbed regions of donor (and acceptor) are required. The perfect situation for this is a bi-layer device with donor and acceptor sandwiched together. A compromise must be found between these two limiting cases. The morphology currently common in organic solar cells is a nanoscale phase separated mixture or donor and acceptor, as shown in Figure 6.

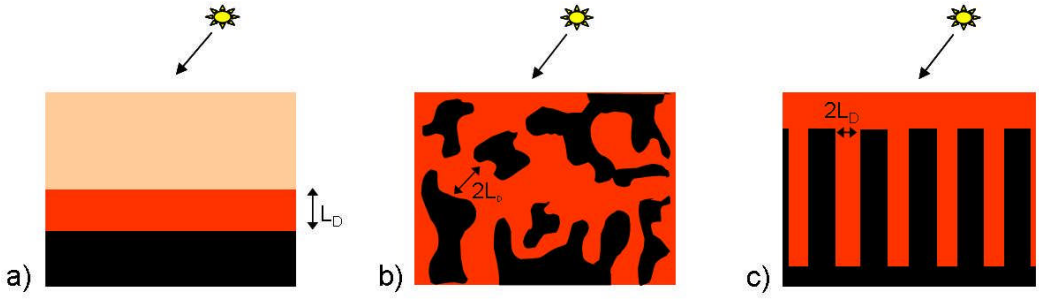

Figure 6. Device structures for organic solar cells. a) a bi-layer device, with acceptor shown in black, active region shown in dark orange and in-active region shown in pale orange b) a bulk heterojunction c) an ideal 'comb-like' structure

An ideal mixture for organic photovoltaics has been suggested by Nelson[18]. An interpenetrating network of ‘comb-like’ donor and acceptor phases would maximise both charge separation and extraction. This would work best if the spacing between fringes was twice the exciton diffusion length. Unfortunately it is not currently possible to manufacture structured devices with widths of tens of nanometers and

lengths of hundreds of nanometers. However, the idea shows the potential for increasing device performance through morphology structuring.

1.4 Photoluminescence Quenching

When excitons are separated, they can no longer produce photoluminescence. Therefore the quenching of photoluminescence can be used to study this important step in device operation. This can be used to determine if the correct morphology is present in a device, or to look at the process of exciton diffusion.

If left alone, the excitons in a material have a natural decay rate, k, determined by the relaxation from the excited state to the ground state. At low exciton densities, this decay rate is largely independent of the number of photoexcitations[19]. The decay rate can be found experimentally by studying the intensity of photoluminescence I(t) as a function of time:

$$I(t) = I_0 e^{-kt} \qquad (1)$$

The initial intensity is I_0. The decay rate can then be expressed as both radiative and non-radiative elements.

$$k = k_r + k_{nr} \qquad (2)$$

For a polymer in solution, the decay is generally monoexponential[19]. However, in film the interaction is complicated by interchain interactions, exciton trapping and aggregate formation. Therefore the decay is best approximated by a sum of weighted exponentials.

$$I(t) = \sum_i A_i e^{-k_i t} \qquad (3)$$

Where A is a weighting factor and $\Sigma_i A_i = 1$. Generally two or three exponentials are required.

The decay rate can also be expressed as a lifetime, τ:

$$\tau = \frac{1}{k} \qquad (3b)$$

The natural decay lifetime can be altered by the presence of an electron acceptor. Excitons are dissociated at the acceptor interface and are unable to contribute to photoluminescence (PL). If good acceptors are present throughout the blend no PL will be observed. If acceptors are present but in a lesser amount a faster PL decay will be noted. This change in decay time can be measured to provide useful information about the effectiveness of a photovoltaic blend, the presence of quenchers, or the movement of excitons[12,20].

1.4.1 Photoluminescence Quantum Yield

Excitons can return to the ground state by emitting a photon, or by non-radiative relaxation. The ratio between these processes is expressed by the photoluminescence quantum yield. This is defined as the number of photons emitted by the samples divided by the number of photons absorbed by the sample (Equation 4a). It can also be defined in terms of the radiative decay rate k_r and the non-radiative decay rate k_{nr}[21] (Equation 4b). Q_0 is the photoluminescence quantum yield. This is an important parameter, particularly as it gives an upper limit on the electroluminescent quantum yield, which is important for light emitting applications.

$$Q_0 = \frac{N_{photons\cdot\cdot emitted}}{N_{photons\cdot\cdot absorbed}} \qquad (4a)$$

$$Q_0 = \frac{k_r}{k_r + k_{nr}} \qquad (4b)$$

1.5 Förster Transfer

1.5.1 The Theory of Förster Transfer

Förster transfer is an important process in polymer photophysics.[22] It describes the radiationless transfer of energy between two dipoles. For this to occur there must be a spectral overlap between the donor's emission spectrum and the acceptor's absorption spectrum. The strength of the interaction depends on this spectral overlap, the distance between donor and acceptor and the relative orientation of the dipoles. The interaction is strongly distance dependent, with an inverse sixth power relationship. The efficiency of transfer, E, for a point-point dipole system is therefore described by

$$E = \frac{1}{1+\left(\frac{r}{R_0}\right)^6} \qquad (5)$$

Where r is the distance between donor and acceptor and R_0 is the Förster radius. The Förster radius is defined as the distance at which half of the energy is transferred from the donor to the acceptor non-radiatively. The Förster radius can be calculated using the following equation[7]

$$R_0^6 = \frac{9Q_0 \ln(10)\kappa^2}{128\pi^6 N_A} \int \frac{f_d(\lambda)\varepsilon_A(\lambda)\lambda^4}{(n(\lambda))^4} d\lambda \qquad (6)$$

Where Q_0 is the fluorescence quantum yield of the donor, κ^2 is the dipole orientation factor, N_A is Avogadro's constant, $f_d(\lambda)$ is the normalised fluorescence of the donor $\varepsilon_A(\lambda)$ is the molar extinction coefficient of the acceptor and $n(\lambda)$ is the refractive index of the material as a function of wavelength, with all quantities in standard units.

A critical concentration of acceptor particles, N_0, corresponding to the Förster radius can be defined as:

$$N_0 = \left[\frac{4\pi R_0^3}{3} \right]^{-1} \qquad (7)$$

An assumption is made that the acceptors occupy a sphere of radius R_0. The Förster equations can be altered for different geometries, such as point to plane transfer. For that geometry, the distance dependence reduces to x^{-3}.[23]

1.5.2 Self Förster Transfer

When there is an overlap between emission and absorption spectra of a molecule, it is possible for Förster transfer to occur between molecules of the same type. Considering a polymer chain, divided into small conjugated sections of different lengths but similar properties, it is easy to imagine an exciton hopping between sections of this chain by Förster transfer. This is believed to be the main method of travel for excitons[24]. If this is true, polymers with a large spectral overlap in their emission and absorption would be expected to have large exciton diffusion lengths. The relative orientation of polymer chains is also important, as demonstrated by Herz et al.[25]

1.6 Crystallinity

Another factor that may affect exciton diffusion length is the crystallinity of the polymer. In the crystalline phase polymer chains stack together to create microscopic rigid structures known as lamella. Packing the chains together is easy if the polymers are highly regular or if the interchain interactions are favourable. If the chains are irregular and with weak or repulsive forces between them, a disordered mixture of polymer chains will be form. This is known as the amorphous phase. Most polymers lie between these two phases, with crystalline sections and amorphous parts mixed together. The balance between these can be altered by the application of heat or pressure and by slowing solvent evaporation rates when preparing from solution.

It is known that increasing the crystallinity of a polymer has astounding effects on the charge transport properties of the polymer[26]. It is likely that this is the reason for the increase in solar cell performance when the polymers used are more crystalline[9].

Recently studies have been made looking at the relationship between crystallinity and exciton diffusion length in small molecule organic semiconductors[27]. More crystalline formations lead to a longer diffusion length. While this area is still being investigated, the likely cause of this is that high crystallinity reduces the interchain separation, allowing self Förster transfer to occur more efficiently. However, this result was for a small molecule system, and the situation in polymers cannot be assumed. For example, the substance MEH-PPV has a much higher exciton diffusion length than P3HT, despite being less crystalline[28].

Chapter 2

Experimental Details

2.1 Materials Used in this Work

The polymers most often used in this work were P3HT and PCBM. The molecular structures of P3HT and PCBM were shown in Figure 4. The P3HT used was supplied by Merck. It had a regio-regularity of 98.5% and a molecular weight of 76,000 $gmol^{-1}$. The batch number was EF430302. The PCBM used was supplied by SES Research. The purity was > 99% and the PCBM was used as supplied. The lot number was PC6-202 and the category number was 910-1500-1. Other materials used in this work are described in the relevant section.

2.2 Steady State Photophysics

2.2.1 Absorbance

Organic materials absorb light in the ultraviolet and visible with an absorbtion spectrum characteristic of the material. The absorbance is also related to the thickness of the sample by the absorption coefficient at any particular wavelength. If the incident light intensity on a sample is I_0, and the transmitted light intensity though the sample is I, then the absorbance is defined as

$$A = -\log_{10}\frac{I}{I_0} \qquad (14)$$

The relationship between absorbance, thickness (d) and absorption coefficient (α) is given by

$$A = \frac{\alpha d}{\log_e(10)} \qquad (15)$$

Absorbance spectra were measured using a Varian Cary 300 UV-Vis Spectrometer, which has a range from 200-900 nm. Before measurement a baseline scan was performed with two blank substrates. During measurement a reference sample was placed in one arm of the spectrometer, with the main sample in the other arm. The absorbance spectrum of P3HT is shown in (Figure 7).

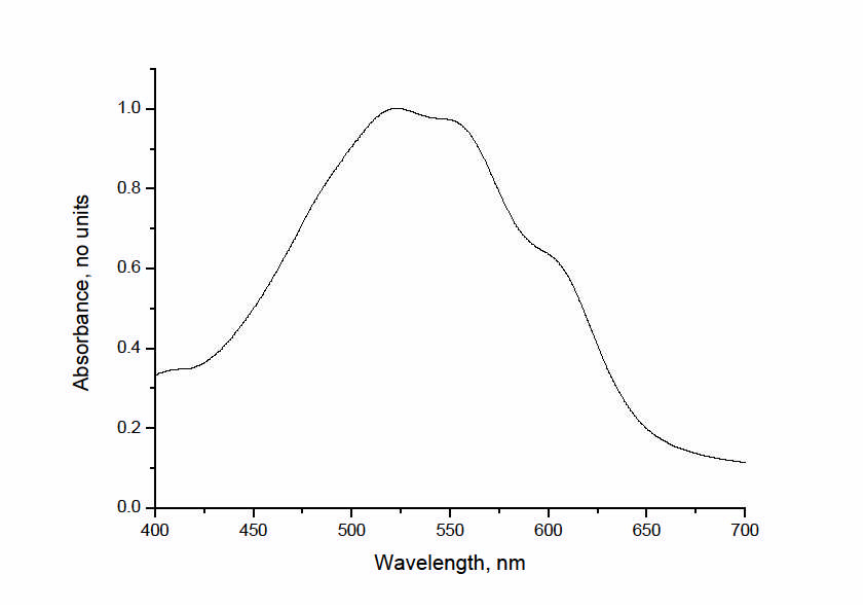

Figure 7. The absorbance spectrum of P3HT

2.2.2 Photoluminescence

The photoluminescence of polymers can also be studied. An appropriate excitation wavelength is chosen and the emission is studied over a broad range of wavelengths. The collected data is corrected using a standard data-set to calibrate for instrument response.

The fluorimeter used was a Horiba Jobin Yvon Fluoromax-2. The photoluminescence of P3HT is shown below (Figure 8). An overlap between P3HT

photoluminescence and absorption occurs between 600-650 nm, so self Förster transfer can occur.

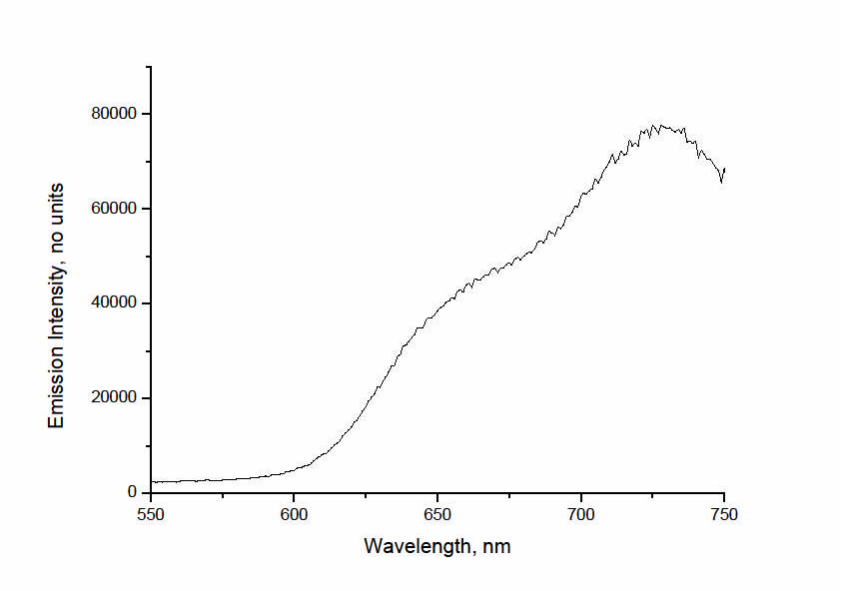

Figure 8. The photoluminescence spectrum of P3HT.

2.3 Time-Resolved Photoluminescence

The following section describes the experimental set-up used for time-resolved fluorescence measurements. It consisted of a femtosecond pulsed laser, frequency doubling crystal and a streak camera. This set up was used for the measurements of surface quenching discussed in Chapters 5,6 and 7 and the measurements of volume quenching of P3HT emission by PCBM domains discussed in Chapter 4.

2.3.1 Femtosecond Pulsed Laser

A femtosecond pulsed laser was used to excite the samples. The system used was a Spectra Physics Mai Tai laser, which produces pulses of 100 fs width with a repetition rate of 80 MHz. The laser can be tuned from 750-850 nm. Two lasers were used within the Mai Tai to create the pulsed beam. A ND:YVO_4 diode-pumped solid state laser pumps the mode locked Ti:Sapphire laser. Mode locking occurs by a combination of acousto-optic modulation and self phase modulation[29].

2.3.2 Streak Camera

Streak cameras are capable of measuring light pulses with picosecond resolution. In combination with a spectrograph, they can simultaneously collect information on wavelength, time and intensity.

A diagram of streak camera operation is shown below (Figure 9). A spectrograph horizontally sorts light by wavelength, which is then incident on the streak camera slit. A photocathode converts the photons to electrons, with the number of electrons proportional to intensity. Each electron is then accelerated through an oscillating electric field. This causes the electrons to be deflected, with deflection varying with time, so the electrons are sorted vertically by arrival time. A micro-channel plate increases the number of electrons, which then strike a phosphor screen. A CCD detector captures the photons emitted from the phosphor, and creates the image containing the necessary data. By integrating the image vertically time-resolved information can be obtained. By integrating horizontally spectral information was obtained.

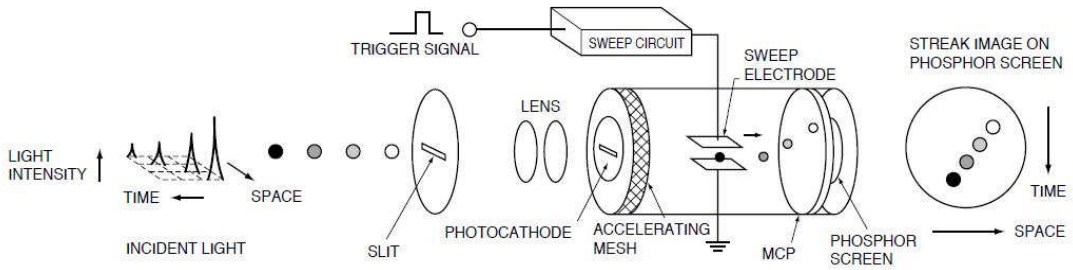

Figure 9. The operation of a streak camera. Diagram from Hamamatsu Guide to Streak Cameras

The time range in which the streak camera collects information can be adjusted by varying the oscillation of the electric field. Various time ranges are available, these are summarised in the table below along with the instrument response function at each time range. The instrument response function was not used as the decays studied are of longer time scale.

	Window, ps	Instrument Response, ps
Range 6	2000	50
Range 5	1000	20
Range 4	500	10
Range 3	200	5
Range 2	100	3.5
Range 1	50	-

Table 1: The time ranges available to the streak camera with their respective resolutions. Time Range 1 was not used.

2.3.3 Experimental Set-Up

The experimental set up for time-resolved photoluminescence measurements is shown below (Figure 10). Pulsed light from the Mai Tai laser was frequency doubled by the BBO crystal. For P3HT an excitation wavelength of 400 nm was used. A blue filter cut out any remaining 800 nm light from the laser. The sample was excited at an angle slightly off normal. This prevented the laser beam from shining directly onto the streak camera, but minimised reflections with near normal incidence. The samples were placed with the polymer side facing the laser beam as it was found that the intensities needed were less in this configuration due to reflections by the TiO_2, The samples were kept under vacuum during measurements.

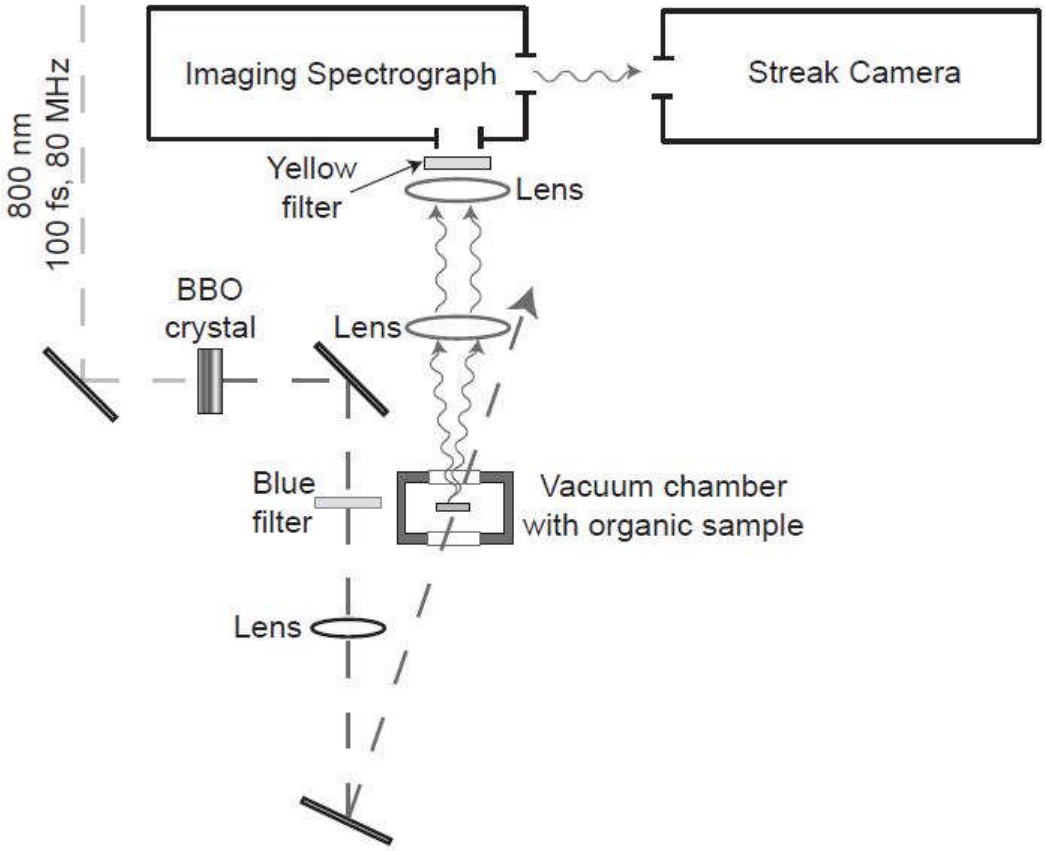

Figure 10. The optical table set-up for time-resolved photoluminescence measurements[19].

The photoemission from the sample was collected using a lens and focused onto the spectrograph slit. A yellow filter removed any remaining excitation wavelength. The intensity of the incident laser was set to ensure excitation densities remained well below annihilation levels. This was done by initially testing the samples at several intensity settings to find an appropriate intensity in the time independent range.

A background reading was taken, and extracted from all data sets. After each measurement the sample position was changed slightly and a vertically integrated profile was recorded to give time-resolved information. Between six and ten measurements were taken. These were then averaged to give a position averaged photoluminescence decay.

2.4 Surface Measurements

2.4.1 Profilometry

Profilometers are used to measure the surface profile of a sample. Thickness information was obtained by scoring the sample with the tip of a metal blade before studying it. The profilometer used was a Veeco Dektak 150. It consists of a small metal tip which was dragged across the surface of the sample. Variations in the surface are recorded and from this a thickness can be measured. A typical profile scan is shown in Figure 11.

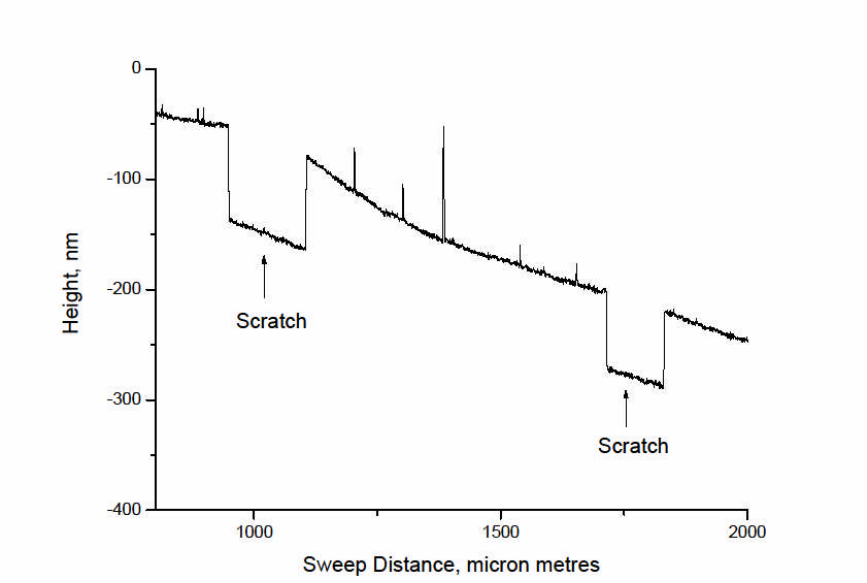

Figure 11. The surface profile of a 75 nm thick superyellow film on quartz.

2.4.2 Atomic Force Microscopy

Atomic force microscopy (AFM) is the most commonly used tool for imaging and measuring nanoscale structure, and gives images of the surface of samples. An AFM consists of a cantilever with a probe tip, a laser beam, photodiode and electronic feedback system. The tip is lowered until it is just above the surface of the sample. Intermolecular forces act on the tip and cause its position to deflect slightly. This deflection is measured with the help of a laser focused on the tip and a photodiode. Electronic feedback mechanisms are used to alter the distance between the tip and sample, to monitor the approach of the tip towards the sample and prevent the tip crashing into the sample.

Two scanning modes are possible with AFM: contact and tapping. In contact mode the force between the tip and sample is kept constant. Contact mode can have problems with noise and deflection, but is preferred for hard samples. Using contact mode on soft samples such as polymers can result in scratching the samples, so tapping mode is preferred. In tapping mode the tip is vibrated close to its resonant frequency. Small changes in the force will produce large changes in the oscillation amplitude. Tapping mode measurements are therefore more sensitive and have produced the best resolution to date.

The image produced from AFM scans must be carefully analysed for image artifacts. Analysis can be performed to extract useful characteristics such as average surface roughness and domain size. The AFM used was a Veeco Caliber. A scan of a titanium dioxide sample such as those used in surface quenching experiments is shown below (Figure 12).

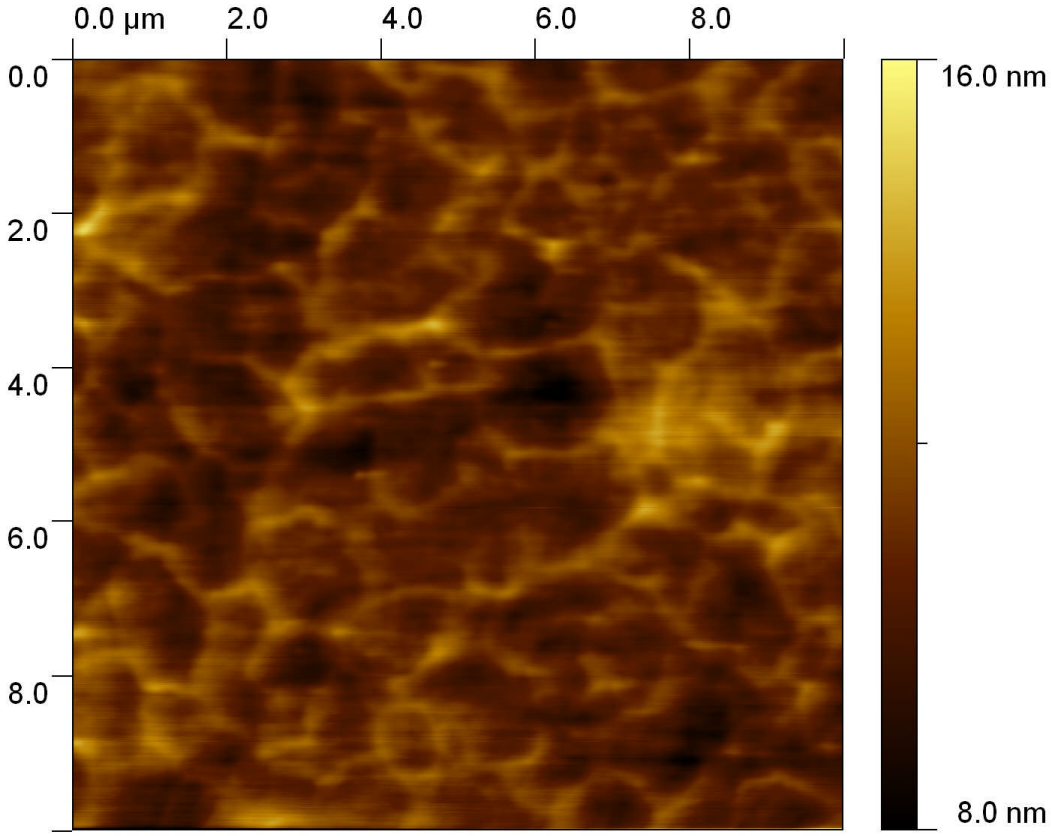

Figure 12. An AFM scan of an 80 nm thick titanium dioxide layer prepared by e-beam evaporation. The average surface roughness of the sample was 0.9 ± 0.1 nm for the 10µm by 10µm region shown

Chapter 3:

Measuring the Optical Constants of P3HT

3.1 Motivation for the Work

To measure the exciton diffusion length of P3HT using surface quenching techniques (discussed in Chapter 5), thin polymer films are required, with the thickness of these films a crucial parameter in the modelling of exciton diffusion through the polymer. It is difficult to measure the thickness of thin P3HT films using methods such as surface profilometry or AFM, as measuring the thickness requires making a scratch and the uneven edges of the scratch obscure useful thickness information. This scratching completely obscures all useful thickness information in thin samples such as those used in surface quenching. Another method is required.

The best method for measuring the thickness of thin polymer films is to use an ellipsometer. Ellipsometry is a complex and beautiful measurement technique which measures the polarisation of light reflected and transmitted by a sample, then uses optical modelling to find the optical constants and thickness of the samples. Both parameters can be fitted simultaneously, though it is preferable to have some information about thickness from another source (eg. profilometry) for some of the thicker films. This is useful for P3HT as it was possible to measure the thickness of several thick films using the profilometer, from which optical constants were found. These optical constants can fit to information for thinner films such as those used in surface quenching experiments. The thickness of these thin films can then be measured, which would be impossible with the profilometer.

This chapter discusses the techniques of ellipsometry and presents measurements of the optical constants of P3HT. These measurements were used to determine the thickness of the samples used in surface quenching later in this work.

3.2 Ellipsometry of Conjugated Polymers

Ellipsometry of conjugated polymers is used to measure the optical properties of the polymer[30,31], the thickness of thin polymer films[19,32] or to estimate the degree of orientation of the molecules within the film[33], though alternative uses have been explored[34],[35]. Wong et al[36] use ellipsometry to confirm the thicknesses of films when testing a new polymer for photovoltaic devices, and also confirm the high absorption co-efficient of the polymer from ellipsometric measurements. Ellipsometric techniques are particularly powerful for measuring the thickness of thin films and the absorption properties of these films, as the measurement of a change in polarisation means that films much thinner than the wavelength of light can be studied[37].

3.3 Theory of the Complex Refractive Index

The complex refractive index of a material is given Equation 16, where n is the phase velocity of light in the material, and k is the extinction co-efficient of light in the material.

$$\tilde{n} = n + ik \qquad (16)$$

The extinction co-efficient can be related to the absorption co-efficient α. The refractive index and extinction co-efficient are related by the Kramers-Kronig relationships[7] given below, with P indicating that the principal part of the integral should be taken.

$$n(\omega) = 1 + \frac{1}{\pi} P \int_{-\infty}^{\infty} \frac{\kappa(\omega')}{\omega' - \omega} d\omega' \qquad (17a)$$

$$\kappa(\omega) = -\frac{1}{\pi} P \int_{-\infty}^{\infty} \frac{n(\omega') - 1}{\omega' - \omega} d\omega' \qquad (17b)$$

Information about the complex refractive index and the thickness of the films is found from ellipsometric modelling.

3.4 Ellipsometric Techniques

An ellipsometer measures the change in the polarisation of a light beam when reflection and transmission measurements are taken. The sample is mounted in a sample holder between two arms of the ellipsometer. One arm holds a light source, and the other holds a photodiode. The sample was placed such that the beam from the light source was reflected from the sample onto the centre of the photodiode. Alignment of the photodiode to ensure the maximum signal was detected was performed. The angle of the ellipsometer arms was then changed between 45° and 75° and measurements of the change in the polarisation of the beam upon reflection were taken. Measurements in transmission mode were also taken, with the arms of the ellipsometer parallel to one another and the sample aligned perpendicular to the arms. The alignment of the sample in transmission mode was checked using a small bubble level, to ensure it was truly perpendicular to the photodiode.

The measured values of the change in polarisation are known as psi and delta. They can be related to the complex reflection and transmission for s and p polarised light as follows:

$$\frac{\hat{R}_p}{\hat{R}_s} = \tan\Psi_R e^{i\Delta_R} \qquad \frac{\hat{T}_p}{\hat{T}_s} = \tan\Psi_T e^{i\Delta_t} \qquad (16)$$

The values measured are independent of amplitude as they are ratios between p and s polarised light measurements. This increases the accuracy of ellipsometry, as it is difficult to ensure that all the light reflected has been detected in amplitude measurements. Psi and delta cannot directly be related to the optical constants, which are found via a fitting process. An optical model is constructed and iterative fits performed to find the best fit to the experimental data. The fitting was performed using the J A Woollam WVASE32 software, which uses a Levenberg-Marquardt algorithm.

The ellipsometer used was a JA Woollam Co., Inc M-200DI spectroscopic ellipsometer. Reflection measurements were performed at several angles, in particular focussing on the range 55° to 60° where the behaviour of psi and delta was seen to change. Transmission measurements were made at normal incidence.

Most polymers are known to have optical anisotropy[31,36,38,39], however this was not considered here as it is not essential for determining film thicknesses. To build an anisotropic model, an isotropic model is first developed, then adjusted to allow fitting for ordinary and extraordinary parts of the optical constants.

For polymers it has been found that the best results are gained by combining reflection and transmission data[38]. Both reflection and transmission measurements were therefore used in the fitting process. Samples used in this work were prepared on fused silica discs, as this is consistent with the substrate used for surface quenching experiments. The optical constants of the fused silica discs had been fitted separately, and were included as part of the model. Reflections within the sample were also considered in the modelling.

3.5 Film Preparation

Four films were prepared by spin-coating from solutions of P3HT in chloroform onto fused silica substrates. The concentrations were in the range 2-10 mg/ml. Spin-coating was performed inside a glovebox to reduce oxygen exposure. The spin speed used was 2000 rpm. This resulted in film thicknesses ranging from 14 nm to 60 nm, giving a selection of thicknesses which could be measured on the profilometer and the ellipsometer. The thickness of the samples was measured using the profilometer, and this measured thickness was included as a parameter in the fitting.

3.6 Results

The experimental data, generated model fit and optical constants for P3HT derived from the model are shown overleaf (Figure 13). The experimental data and model fit are shown at several different angles. A good fit can be seen between the experimental data and model. The model consists of two gaussian peaks and was built up using four different samples. Gaussian oscillators were used to construct the model, with each oscillator representing an optical transition within the polymer, which is a physically sensible model of the optical properties. The parameters fit are the strength of the oscillator, the frequency at which maximum oscillation occurs and the breadth of the oscillator.

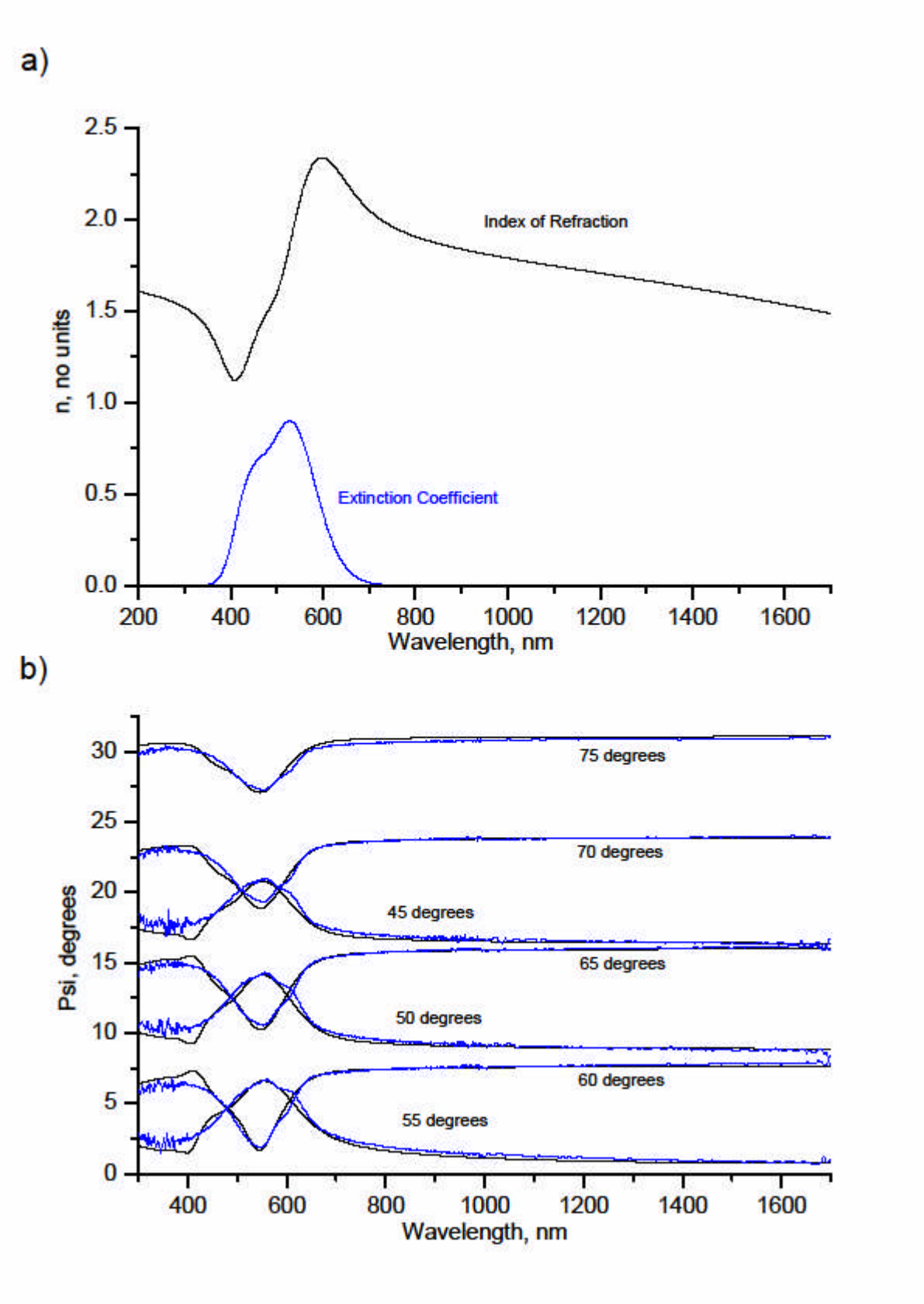

Figure 13. Ellipsometric modelling of Merck P3HT. The optical constants are shown in a). The model consists of two Gaussian peaks and was built up using four different samples. The experimental data and generated model fit are shown in b), with colours blue and black respectively. The MSE of the fit was 22. It can be seen that the fit could be improved, particularly for the 600 nm shoulder. However, to do so would require more Gaussian peaks.

The optical constants from the fitting are physically reasonable, with the extinction coefficient value corresponding to the absorbance spectrum of P3HT. At 540 nm, the extinction co-efficient of 0.878 is equivalent to an absorption co-efficient of 20,436,959 m^{-1}. For a 9 nm thick film, this equates to an absorbance of 0.0798. The absorbance of a 9 nm thick film was measured to be 0.0803. This shows that the extinction co-efficient is correctly scaled.

The index of refraction is high as expected for a polymer, with a noticeable deviation where the extinction coefficient is highest. The optical constants produced were smooth and continuous, another sign that a physically reasonable model has been found. The mean square error of the fit was 22, which is comparable to the MSE of 50 found by Ramsdale et al for an isotropic polymer ellipsometeric model[38]. The fit could be improved, particularly for the 600 nm shoulder. However, to do so would require more fitting parameters, which reduces the physical simplicity of the model.

Thin samples (~14 nm) were also included in the modelling to ensure that the same optical constants could sensibly be used for both thick and thin samples. This is important as some authors have proposed that there could be a change in morphology in thin polymer films[11]. This could lead to a change in the optical properties. In this work, no difference in the optical properties of thick and thin P3HT samples was observed. The developed model could therefore be applied to thin samples such as those used in surface quenching measurements with confidence.

3.7 Thickness Measurements of Thin Polymer Films

The ellipsometric model developed in this chapter was used to measure the thicknesses of P3HT films used in measurements in later chapters. Reflection and transmission measurements were made for each sample. The model of the optical properties was then fitted with film thickness as the only parameter. This model gave a reliable method for measuring the thickness of thin films; which is consistent with other work reported in the literature[36,40] that has found ellipsometry to present a robust measurement of film thicknesses. Film thicknesses were measured with

accuracy ± 0.5 nm, which is acceptable for determination of diffusion co-efficients through surface quenching. Ellipsometric techniques contrasts with other measurement techniques, such as absorbance measurements, which are often affected by problems with reflection[41]. This technique of measuring thin film thicknesses through ellipsometry is important as it allows the very thin films to be measured accurately, which is essential for surface quenching measurement techniques[19].

Chapter 4

Morphology Studies using Low Concentration Volume Quenching

4.1 Basis for the Work

Morphology studies are of great interest in organic solar cells. Only by finding the optimum morphology will the best device efficiencies be achieved. Morphology can be affected by "thermodynamic" characteristics such as the materials used and their interactions and solubility, or by "kinetic" parameters such as the solvent evaporation rate, crystallisation and annealing rate[42].

Morphology studies become particularly interesting when additional information can be acquired at the nanometer scale. The nature of domains, the crystallinity of the materials and local photoluminescence quenching give greater insight into the effectiveness of a photovoltaic blend[43].

One of the challenges of understanding morphology is the difficulty of measuring on the nanometer scale. Atomic force microscopes can provide excellent information with a resolution of ~10 nm, but are only suitable for studying the surface structure. Transmission electron microscopy is another technique producing interesting information, yet provides a projected image of the 3-D structure[11,44]. Studies of the time-resolved decay of polymer blends are therefore particularly useful as they can give insight into the 3-D structure of the film. Where structural information is available, time-resolved studies give important information about how photophysics relates to structure.

Ruseckas et al[20] looked at energy transfer in P3HT:PCBM blends through time-resolved fluorescence measurements. They observed quenching caused by nanoscale PCBM domains. Quenching occurred by a combination of exciton diffusion and Förster transfer. The dynamics of Förster transfer alone are described by

$$g(t) = g(0)\exp\left[-\left(\frac{N_m}{N_0}\right)\left(\frac{\pi t}{\tau}\right)^{\frac{1}{2}}\right] \qquad (11)$$

where N_m is concentration of acceptor molecules, N_0 is the critical concentration for Förster transfer, g(t) is the fluorescence intensity ratio and τ is the fluorescence decay time of films without PCBM present. The Förster transfer radius was found to be 1.2 nm by fitting this equation to data collected for a 90 wt% blend of PCBM in P3HT.

Building from this knowledge, the fluorescence decay by exciton diffusion and Förster transfer was considered. The fluorescence intensity as a function of time I(t) can be described by Equation 12 in which I_0 is the intensity of t=0 and $k_q(t)$ is the quenching rate by PCBM. The quenching rate is described by Equation 13, where D is the diffusion coefficient found from earlier work, R_c is the exciton capture radius and N_d is the concentration of the quencher.

$$I(t) = I_0\exp\left[-\left(\frac{t}{\tau}\right) - k_q(t)t\right] \qquad (12)$$

$$k_q = 4\pi D R_c N_d \left(1 + \frac{R_c}{\sqrt{\pi D t}}\right) \quad (13)$$

At long time scales, the behaviour of k_q is time-independent. This was verified by Ruseckas et al. This then simplifies equation 13 to

$$k_q = 4\pi D \cdot R_c \cdot N_d \quad (14)$$

To find the size of the PCBM domains, the mass of PCBM in small domains was considered. This can be found by looking at the fraction of PCBM in the blend, f, the fraction of PCBM stored in small domains, s, and the film density within these domains, ρ, as seen in equation 15b. It can also be found by assuming the domains are spherical with radius r, as shown in Equation 15b. By equating 15a and 15b, the expression for N_d in Equation 14 can be substituted out.

$$m = s \cdot f \cdot \rho \quad (15a)$$

$$m = \rho \cdot (4/3)\, \pi\, r^3 \cdot N_d \quad (15b)$$

$$R_c = r + d \quad (15c)$$

This then leaves only the exciton capture radius, R_c as an unknown quantity. This can be found by equating the exciton capture radius with the domain radius, r, and d, the Förster radius (Equation 15c). The value of d was found to be 0.6 nm in work by Ruseckas et al, and this value is used here. Assuming that all PCBM is contained within domains (s=1) and combining Equations 15a-c with Equation 14, gives Equation 16, which has only one unknown parameter, r, the domain size.

$$k_q = 3D(r+d)f \cdot r^{-3} \quad (16)$$

By finding k_q from the experimental data, the domain size could be found for PCBM:P3HT blends of different concentrations. This is a powerful method to measure the size of PCBM domains to within 1 nm. This level of precision is not possible with other techniques investigating morphology.

Using this methodology, Ruseckas et al found a domain size of 9.4 nm for a 50 wt% blend of P3HT and PCBM, which corresponds well to other measurements. For a 10 wt% ratio the domain size was 5.6 nm. For a 2 wt% blend the domain size was 4.6 nm. These results show a consistent trend of decreasing domain size with decreasing PCBM fraction.

In my work I developed this approach and explored the behaviour of P3HT doped with very small concentrations of PCBM. For comparison to the work of Ruseckas et al, some higher concentrations were also studied to ensure an overlap.

4.2 Film Preparation

To achieve small PCBM domains, P3HT solutions with a small percentage of PCBM were prepared. The P3HT and PCBM used are mentioned in Section 2.1. Solutions were prepared in chlorobenzene from PCBM weight percentages of 10% down to 0.01%. The concentration of P3HT was 12 mg/ml. This was kept constant to ensure the thickness of the film was the same for all samples, reducing the chance of any variations in decay time due to difference in film thickness occurring (see Chapter 7 for more discussion). This approach is acceptable for the low doping concentrations used here.

For the very low doping concentrations (< 1% PCBM) serial dilutions of PCBM solutions were used. A solution of 0.6 mg/ml PCBM in chlorobenzene was prepared. This was heated to 40 °C and stirred overnight. 50 µl of this solution were then taken and added to 2450 µl of chlorobenzene to give a solution of concentration 0.012 mg/ml. This was again heated and stirred to allow the PCBM to thoroughly disperse.

The absorbance of these two solutions was measured with the Cary spectrophotometer and compared. The absorbance of the 0.6 mg/ml solution was found to be 50 times greater than that of the 0.012 mg/ml solution, as expected. Solutions of P3HT and PCBM were then prepared according to the weights shown in Table 2. The approach taken was to weigh the P3HT in a small vial, add the appropriate amount of PCBM solution to the vial then to add extra chlorobenzene if required to give the correct concentration.

PCBM % weight	Amount of P3HT, mg	Amount of PCBM solution added, µl of mg/ml solution	Amount of Chlorobenzene added, µl
5%	3 mg	250 µl of 0.6 mg/ml	Nil
2%	3 mg	100 µl of 0.6 mg/ml	150 µl
1%	3 mg	50 µl of 0.6 mg/ml	200 µl
0.1%	3 mg	250 µl of 0.012 mg/ml	Nil
0.01%	3 mg	25 µl of 0.012 mg/ml	225 µl

Table 2: The amounts of PCBM solution and weights of P3HT used in the preparation of the solutions of P3HT doped with small amounts of PCBM.

Once prepared, the PCBM:P3HT solutions were left to dissolve for several hours, with a magnetic stirrer used to facilitate the P3HT dissolving. To create samples, fused silica discs were used as a substrate. These were cleaned with acetone, IPA and chlorobenzene before use. Spin-coating was performed at 900 rpm inside a glovebox. The film thicknesses were around 70 nm, which gave a strong PL signal even under weak illumination.

4.3 Results

The PL decays measured, normalised PL decays with fits to the gradient and calculated domain sizes are shown in Figure 14. For the 5 wt% blend, the reduction in PL when PCBM is introduced can clearly be seen in comparison to the reference sample. This demonstrates that the PCBM present in the blend has quenched excitons through electron transfer. This is observed as a reduction in the PL decay, and an increase in the decay rate. The PL decay was normalised with respect to the pure P3HT reference sample shown in solid black in Figure 14a. Figure 14b shows the ratio of the PL decays of the doped films to the PL decay of the reference sample plotted on an exponential scale. This can then be compared Equation 13. The gradient of the graph is k_q. The time-dependence of k_q can be seen at times less than 150 ps. The gradient is time-independent at longer time scales, as would be expected from Equation 13. Fitting the decay at longer time scales to find the gradient, the domain size was found to be 5.7 ± 0.6 nm. This is slightly larger than the 5.6 nm domain size found for a 10 wt% PCBM:P3HT blend by Ruseckas et al. However, the results are very similar.

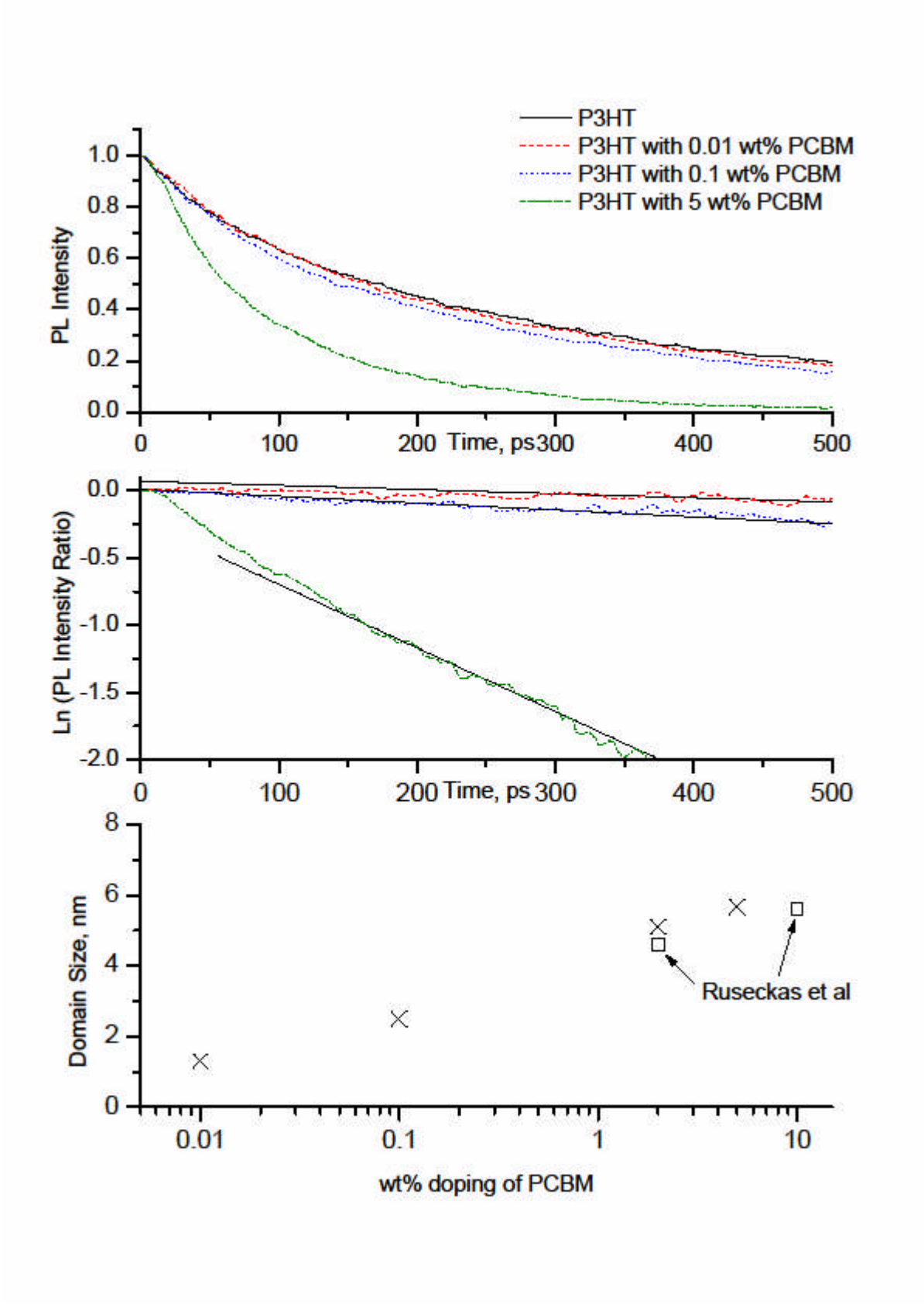

Figure 14. Volume Quenching of P3HT by PCBM. The normalised photoluminescence as a function of time is shown in a). The photoluminscence intensity ratio compared to the pure polymer film is shown in b). The fits are linear. The gradient of the data gives kq. The size of PCBM domains at each concentration is shown in c)

a)

A 2 wt% PCBM:P3HT blend was also studied. The PL decays for this blend are not presented here, as they were collected in a different time range with a different reference sample. Similar fitting procedures were used, and the goodness of fit for the quenching rate was greater than 0.9. Using the same approach, the domain size found for this blend was 4.3 ± 0.4 nm, which is very similar to the domain size of 4.6 nm found by Ruseckas et al for the same doping concentration. The results for the 5 wt% and 2 wt% blends demonstrate the reproducibility of the results of Ruseckas et al.

Extending these results to lower concentrations, the domain size is expected to decrease. There will be a lower limit to the domain size of the size of a PCBM molecule, which is approximately 0.6 nm.

Studying the 0.1 wt% doped sample, the PL decay also shows quenching compared to the reference sample. Here the PL decay is more similar to the reference decay than to the decay of the 5 wt% PCBM sample. This is expected, as there is less PCBM in the blend to quench excitons. Fitting the normalised decay gave a domain size of 1.25 ± 0.1 nm. As expected, this is smaller than the domain size found for the 2 wt% blend.

It also can be seen that there is a very small difference between the unquenched reference sample and the 0.01% doped sample. A 0.01 wt% doping concentration is equivalent to one PCBM molecule for every 110,000 repeat units in the P3HT, so it is quite remarkable that any quenching is observed at all. If a smaller doping concentration was used it is likely that no difference would be observed. Normalising this decay and fitting to the gradient gave a domain size of 1.2 nm. Due to the very small difference between the reference sample and the 0.01 wt% sample's PL decay, this result was repeated. A domain size of 1.4 nm was found when the measurement was repeated. As the errors of the measurement are 10%, these values are within error bars of one another. This domain size is approaching the size of a PCBM molecule, suggesting that the PCBM is molecularly dispersed.

The sensitivity of the measurements to errors was investigated. The main source of error in this measurement was found to be the concentration of the PCBM molecule in the P3HT, as the accuracy of the weighing scales used is 0.1 mg, and measurements of 1mg were required. This contributed a 10% error to all the

measurements, outweighing other possible errors such as finding the gradient of the results in Figure 14b.

The domain sizes are plotted in Figure 14c. A clear trend can be seen, with the domain size increasing with the concentration of PCBM. The results show good agreement with the domain sizes measured by Ruseckas et al (shown with black squares in Figure 14c), and extend these measurements into a lower concentration regime.

4.4 Discussion and Conclusion

The results presented demonstrate that volume quenching of P3HT by PCBM is possible at very low doping concentrations. A clear relationship between the doping concentration of PCBM and the size of the PCBM domains is demonstrated. In addition, the possibility to measure domains of a few nanometre size is shown. This would be impossible with measurement techniques such as AFM, which are better at measuring domains of tens of nanometre size. This shows the strength of PCBM as a quencher, and the capabilities of time-resolved PL measurements as a tool for looking at solar cell blends.

A possible extension of this work is to develop more measurements in the low concentration range, to look for a regime where the PCBM in molecularly dispersed. This could be difficult, as demonstrated by the small difference in PL quenching between the reference sample and the 0.01 wt% PCBM doped sample. If a regime could be found where the domain size remains constant, ie the PCBM is uniformly dispersed as single molecules then it should be possible to deduce the exciton diffusion length from the quenching rate using Equation 16.

Chapter 5:

Exciton Diffusion Measurements using Titanium Dioxide as a Quencher

5.1 Motivation for this Work

Exciton diffusion is an important step in the operation of an organic solar cell as excitons must move from where they are created to a donor acceptor interface where they can be split. Excitons which do not reach the interface will not contribute to the photocurrent. In a bulk heterojunction solar cell, the intermixed layers of donor and acceptor enable this process by reducing the distance that an exciton must diffuse, and increasing the interface area. The optimum condition for these factors is when the phase separation is equal to twice the exciton diffusion length. Accurate knowledge of the exciton diffusion length is therefore important for improvement of organic solar cells.

A further area of interest is the factors controlling exciton diffusion. Areas which would be particularly interesting to investigate include the effect of molecular weight, solvent and annealing. Insight into whether self Förster transfer affects exciton diffusion and whether exciton diffusion is anisotropic could also be gained. It could be possible to maximise the diffusion length, allowing new device structures to be created. This would also allow insight into the complex interplay between exciton diffusion and morphology.

5.2 Previous Work on Measuring Exciton Diffusion

Exciton diffusion can be measured by a variety of methods, including surface quenching[23,45,46] , volume quenching[47,48], microwave conductivity[49], exciton-exciton annihilation[50] and photocurrent modelling of devices[14]. A common factor in exciton diffusion measurements is the presence of a quenching mechanism which destroys excitons. A comparison is then made between a quenched sample and an unquenched sample to find information about the movement of excitons. A problem with these measurements is that the quencher must accept all excitons: a perfect quencher. Incomplete quenching would result in underestimation of the exciton diffusion length.

Surface quenching measurements are the most commonly used, in which a quenching layer is applied. The amount of quenching can then be compared to a reference sample. For steady state measurements the optical field within the sample can be modelled to give information about the exciton diffusion length[33]. For time-resolved measurements exciton dynamics can be modelled, given knowledge of the physical dimensions of the system. Steady state measurements rely on absolute measurements of intensity, so great care must be taken with reflections and interference effects. In contrast, time-resolved measurements compare the photoluminescence decay time, taking advantage of the intensity-independence of PL decay time. This reduces the possibility of errors in the measurement of intensity, but requires specialised equipment as the time scale of exciton diffusion is in the picosecond regime.

Previous studies of exciton diffusion in P3HT include the work of Kroeze[49] and Luer[47]. Kroeze et al used time-resolved microwave conductivity to measure a value of 2.6-5.3 nm, with the broad range due to possible reflections at the polymer/air interface. Oxygen induced fluorescence quenching is used by Luer et al to obtain a minimum value of 4 nm.

Scully and McGehee 2006[23] used a surface quenching approach to make exciton diffusion measurements in MDMO-PPV. They investigated the effects of interference and energy transfer. They used an experimental set up which looks at how the luminescence intensity of quenched and un-quenched substrates changed with polymer film thickness. Titanium dioxide was used as the quencher, with samples prepared by a sol-gel method. They investigated the effect of interference on absolute intensity measurements and find that it can be so prevalent as to obscure results. Interference can be minimised by using 5 nm of titania as a quenching layer. They also consider the effect of energy transfer upon quenching measurements. They quantified the effect of this by including a Förster term in the exciton continuity modelling. This term has x^{-3} distance dependence, as appropriate for a 2-D plane quencher. The inclusion of the Förster transfer process gives additional parameters to the modelling. Scully and McGehee concluded that energy transfer effects are often responsible for an overestimation in the exciton diffusion length.

5.2.1 Time-resolved Measurements

Shaw, Ruseckas and Samuel improve on previous exciton diffusion measurements in their 2008 paper.[12] They used time-resolved fluorescence measurements to find the photoluminescence decay of quenched and un-quenched P3HT samples. By comparing these and modelling the data a diffusion coefficient was found. From this the exciton diffusion length could be calculated. The main advantage of time-resolved measurements is that absolute intensity measurements are not required, as the decay time is independent of incident intensity.

For time-resolved fluorescence measurements they used a femtosecond pulsed laser combined with a streak camera. The quencher used was 80 nm thick layers of titanium dioxide prepared by electron beam evaporation onto fused silica discs. Titanium dioxide was used as it as an effective electron acceptor and forms stable, well defined interfaces. The thickness of titanium dioxide was chosen after optical modelling of the system, as the initial excitation was constant throughout the polymer film. Fused silica substrates were used for the un-quenched decay lifetime.

The modelling uses a one dimensional diffusion equation, shown below. The exciton distribution is described by n(z,t), where t is time and z is the distance from the polymer/vacuum interface. The natural decay of excitons is described by k(t), which is found from the unquenched reference sample. Therefore the only parameter to be found in the modelling was D, the diffusion coefficient.

$$\frac{\partial n(z,t)}{\partial t} = D\frac{\partial^2 n(z,t)}{\partial z^2} - k(t)n(z,t) \qquad (8)$$

In the modelling, a boundary condition was enforced that the population of excitons is zero at the quenching surface. This is valid if the quencher is a perfect acceptor of electrons. The boundary between the polymer and the vacuum was considered to be a perfect reflector of excitons, giving the other boundary condition. The initial distribution of excitons is also important to the modelling, this was investigated using electric field modelling. The thickness of the P3HT films was found using a combination of absorbance measurements and ellipsometry. Measurements were made for several different thicknesses of P3HT film. It was important to have a reference at each thickness as the PL decay is highly dependent on thickness. The same diffusion coefficient of $(1.8 \pm 0.3) \times 10^{-3} cm^2 s^{-1}$ was found for all thicknesses. This shows the robustness of this approach to measuring exciton diffusion coefficients.

From the diffusion coefficient, the exciton diffusion length L_D can be found as follows:

$$L_D = \sqrt{D\tau} \qquad (9)$$

In which τ is the photoluminescence decay lifetime of P3HT. This was found to be 400 ps for thick films. Using this value the exciton diffusion length is reported as (8.5 ± 0.7) nm.

5.3 Experiment

Surface quenching measurements were made following the method of Shaw et al. The time-resolved photoluminescence set-up used was described in Chapter 2. Modelling of the results was performed using the approach developed by Shaw. The model follows the 1-D diffusion equation discussed in the literature section, with the boundary conditions mentioned of a perfectly quenching interface and a perfectly reflecting interface. The equation was solved using a Mathematica program, the results of which were fitted to the experimental data.

5.3.1 Film Preparation

The basis for extending the work is reliably repeating the experiments. All experimental variables were kept as close as possible to those used by Shaw et al. Merck P3HT was used, with a regioregularity of 98.5 %, molecular weight 76,000 g mol^{-1} and a polydispersity of 2.1. Solutions of the polymer were made with chloroform and stirred overnight with heating to 40 °C. The P3HT solutions were cooled before spin-coating. Spin-coating was done at 2000 rpm, Ramp 50, Dwell 60. Generally a 2 mg/ml solution was used, as this creates films of 10 ± 1 nm in thickness. This thickness was found to be ideal for testing, as enough PL is gathered for a reasonable signal to noise ratio at low intensities, yet significant quenching should occur.

5.3.2 Preparation of Titanium Dioxide

Titanium dioxide coated samples can be prepared using several techniques: doctor blading of a titania paste, electron beam evaporation, spray pyrolysis and sol-gel deposition being the most commonly used. The technique used in this work is electron-beam evaporation. Electron-beam evaporation is performed under high vacuum. Electrons are excited from a charged tungsten filament and directed towards a crucible filled with titanium dioxide. This causes the titanium dioxide to evaporate and cover all objects within line of sight. The thickness of the deposited layer is measured by a vibrating quartz crystal. The evaporation rate can be controlled using the position of the electron beam, the frequency of oscillation of the electron beam and the current applied to the tungsten filament.

During evaporation a deposition rate of 0.1 nm/s was preferred, however rates of 0.03 nm/s were generally achieved. After evaporation the titanium dioxide coated substrates were heated to 450 °C for one hour to allow the anatase formation to dominate. The samples were cleaned after sintering, using acetone and IPA.

5.4 Problems with Titanium Dioxide as a Quencher

It was often found that titanium dioxide did not quench effectively. Results are shown below (Figure 15) for an 11 nm thick layer of P3HT on both fused silica substrates and titania coated substrates, with fits to the experimental data. It can be seen that the PL decay on the titania substrates is slightly faster than on the silica discs. This is due to exciton quenching. The fit to the fused silica substrate was found using three exponential decays. The time constants of these were 18 ps, 90 ps and 300 ps with amplitude 0.2, 0.4 and 0.4 respectively. This provides the natural PL decay of the P3HT at this thickness for use in the diffusion coefficient modelling.

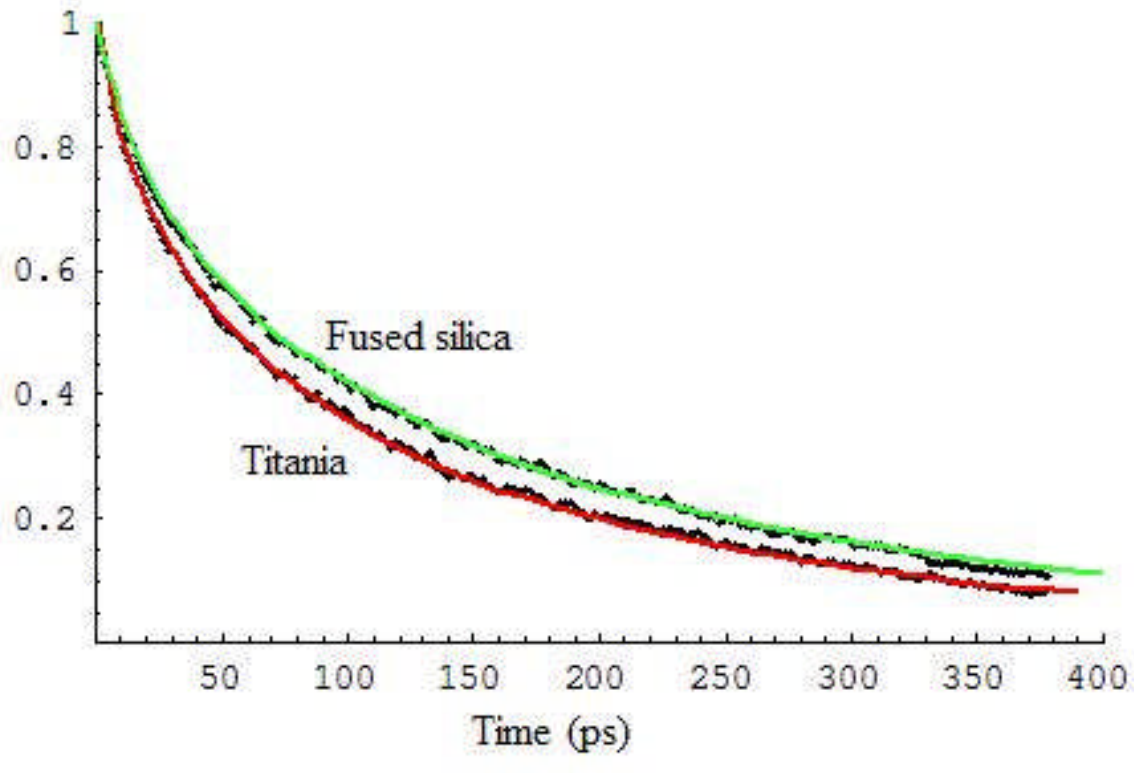

Figure 15. The photoluminescent decay of and 11 nm thick layer of P3HT on fused silica substrates and titanium dioxide covered substrates. The PL decay is averaged over several readings, then normalised. The fit to the fused silica substrate was found manually to give the natural decay of the polymer. The fit to the titanium dioxide sample is based on the one dimensional diffusion equation discussed earlier. The diffusion co-efficient found in the fitting is 2 * 10^{-4} cm^2s^{-1}.

The fit to the titania coated substrate was found using Mathematica code developed by Paul Shaw. This uses the one dimensional diffusion equation discussed in the literature section. The diffusion coefficient found from the modelling is 2.0×10^{-4} cm^2s^{-1}. This is a factor of ten smaller than the value found by Shaw et al. Errors are not quoted for the surface quenching measurement, as the greatest source of error is the quenching strength of the titanium dioxide, which is the parameter under investigation.

By comparing the exciton diffusion coefficient with that found by Shaw et al it is obvious that reduced quenching is being observed. For an 11 nm thick film, a large proportion of the excitons should be quenched. This is a problem as perfect quenching is the most important boundary condition used in the modelling. The quenching experienced by the polymer must be consistent and repeatable for a robust measurement of the exciton diffusion length to be made.

The experiment was repeated many times, often with no quenching observed, as shown in Figure 16. All conditions of the experiment were checked and confirmed as being as close as possible to those used in the work of Shaw et al.

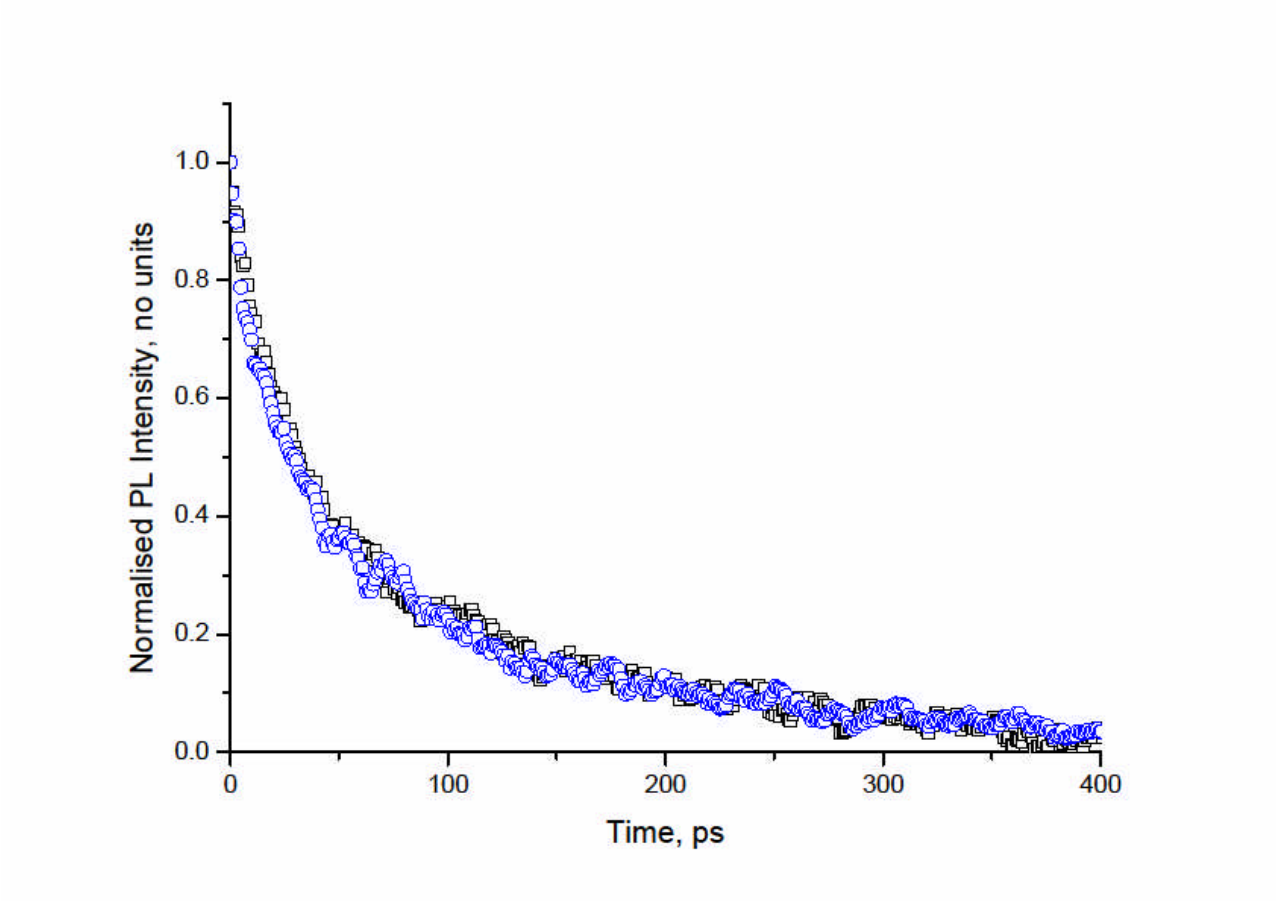

Figure 16. The PL decay of an 11 nm thick layer of P3HT on fused silica (hollow squares) and TiO2 (hollow circles). No difference in PL decay can be observed.

The thickness of the polymer film is important as thin films have faster decay times than thicker films. This will be discussed in more detail in Chapter 7. It is possible that a thickness difference between the reference and quenched sample could account for the observed results. For instance, if the reference sample was much thinner than the quenched sample it is possible that no difference in PL decay would be observed even though exciton quenching had occurred. To check for this, thickness measurements were made with the ellipsometer of P3HT on fused silica substrates and titanium dioxide coated substrates. The polymer thicknesses were found to be within 1 nm of each other on the fused silica and TiO_2 samples. This small difference in thickness is not enough to account for the large observed difference in the quenching in comparison to the work of Shaw et al.

5.4.1 Changing the Preparation Conditions of the Titanium Dioxide

As the movement of electrons from the polymer to the titanium dioxide occurs at the interface between the two, it is likely that this process is highly sensitive to the

properties of the titanium dioxide surface. Experiments were therefore made to investigate whether the titanium dioxide surface is the reason for the lack of PL quenching observed.

The rms average roughness of a 10 μm sample area of the titanium dioxide was measured with an AFM, and found to be 1 nm, similar to that used in the Shaw paper (results shown in Chapter 2, Figure 12).

To check for contamination in the titanium dioxide energy dispersive x-ray spectroscopy was performed, with the help of Ross Blackley. This technique uses a beam of electrons to excite the sample, and collects the x-ray radiation which is produced. From this the characteristic peaks of elements can be observed. Unfortunately overcharging occurred due to the high intensities needed and it was not possible to obtain a clear picture of the elements present in the samples.

To ensure contamination was not an issue a new crucible was bought, and fresh TiO_2 used for evaporations. The results with new TiO_2 are shown in Figure 17. The PL decay of the P3HT observed is slightly slower on the TiO_2 coated substrate than on the reference fused silica substrate. The reason for this anomaly is unknown, however it could be due to a slight thickness difference between the polymer films.

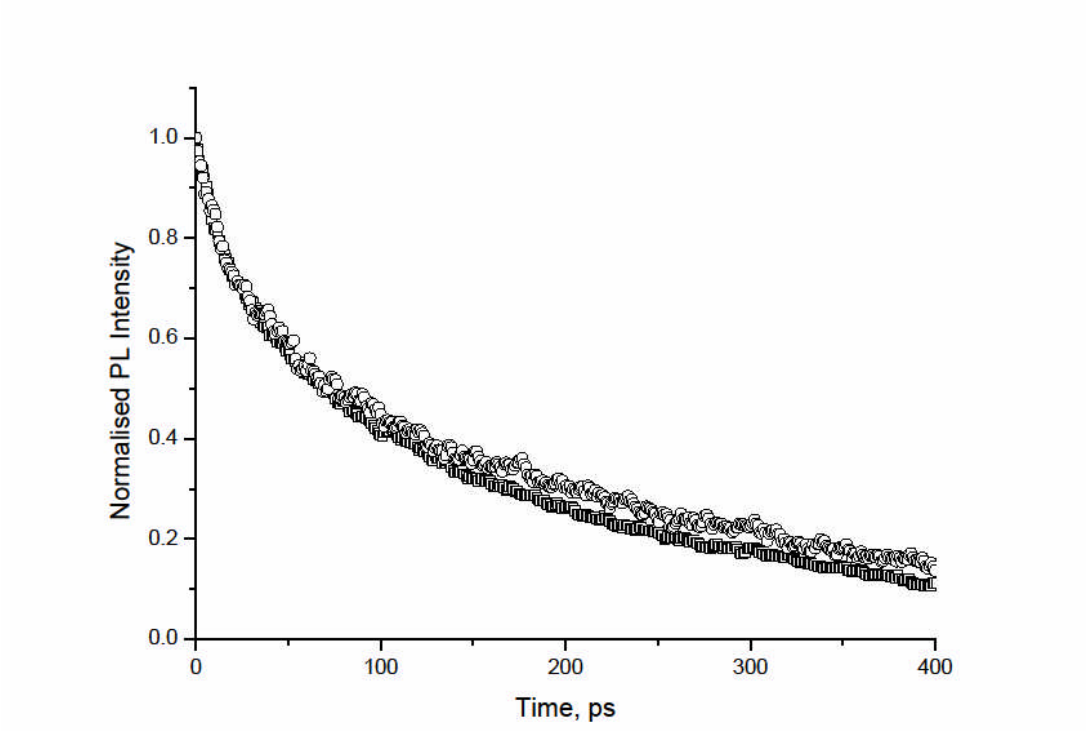

Figure 17. The photoluminescence decay of a 16 nm thick P3HT film on fused silica substrates (hollow squares) and TiO2 (hollow circles). The TiO2 was prepared with a new crucible and new material. The PL decay of the P3HT is slightly faster on the TiO2. This is likely due to a small thickness difference between the polymer films.

The preparation conditions used for the titanium dioxide were varied to see if this affected the amount of quenching. The conditions used by Shaw et al were sintering at 450 °C for one hour, followed by cleaning in acetone and IPA. These conditions were varied to look for a change in PL decay. Figure 18 shows the PL decay of P3HT on TiO_2 which had been sintered, and TiO_2 which had not been sintered compared to a quartz reference. No difference in the PL decay of P3HT is observed between the sample on a fused silica substrate or a sintered and unsintered titanium dioxide coated substrate.

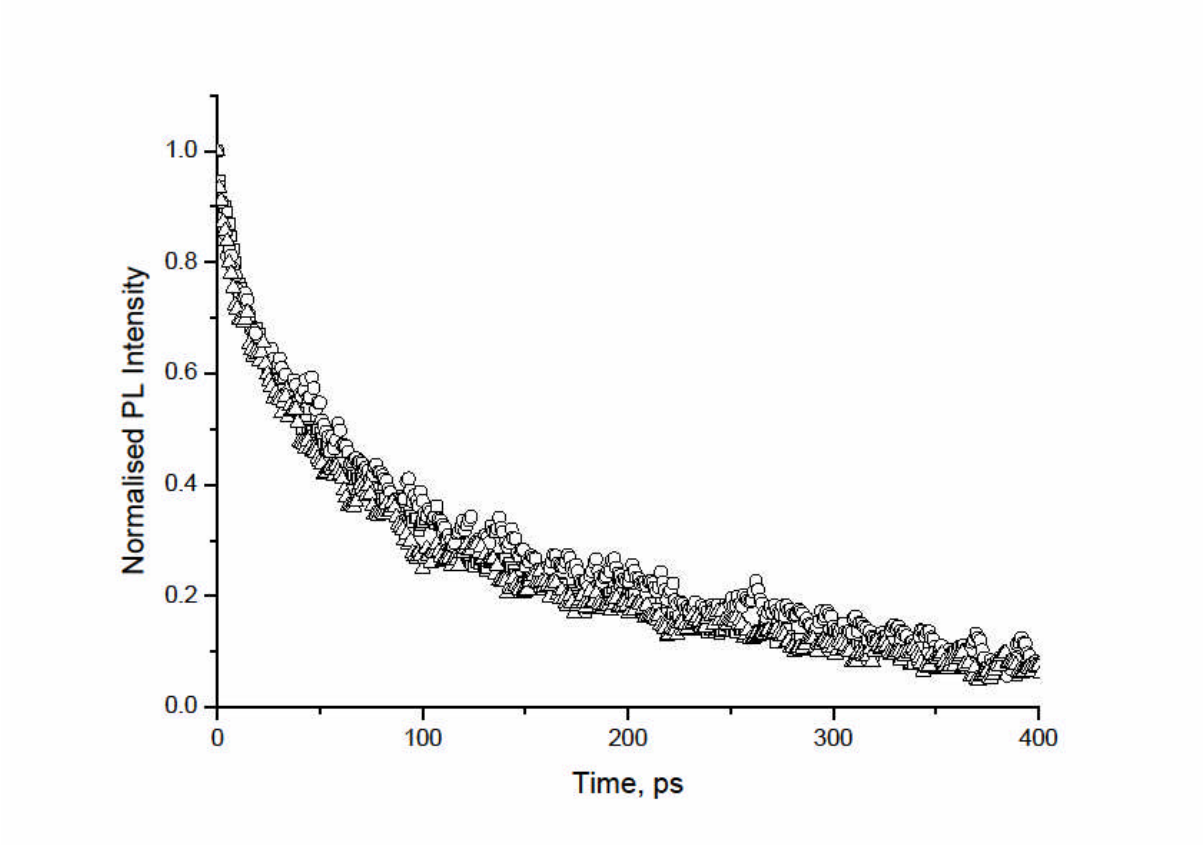

Figure 18. The PL decay of 35 nm thick P3HT films on fused silica (hollow squares), sintered TiO2 (hollow circles) and un-sintered TiO2 (hollow triangles). The TiO2 substrates were cleaned for three minutes in acetone and IPA. No change in PL decay can be seen.

The thickness of the titanium dioxide layer was checked using the ellipsometer. A model for the optical constants had previously been developed by Paul Shaw. This model provided reasonable fits to the data collected for new samples and confirmed that the thickness was 80 ± 3 nm. The thickness of the titanium dioxide layer is important as this can affect the optical field within the polymer[23].

5.5 Surface Treatment of Titanium Dioxide

It has previously been shown that treating the surface of the titanium dioxide with a small molecule can improve the transfer of electrons from P3HT to the titanium dioxide[46]. The most effective surface modifier found is a ruthenium dye known as N3, which is commonly used in dye sensitised solar cells. N3 facilitates the movement of electrons from P3HT to titanium dioxide in two ways. The LUMO of N3 is at 3.9 eV, which lies between the LUMO of P3HT and titanium dioxide. This allows electrons to jump from the LUMO of the P3HT to the LUMO of the N3 before moving to the titanium dioxide. The structure of N3 and the relevant LUMO levels can be seen below in Figure 20.

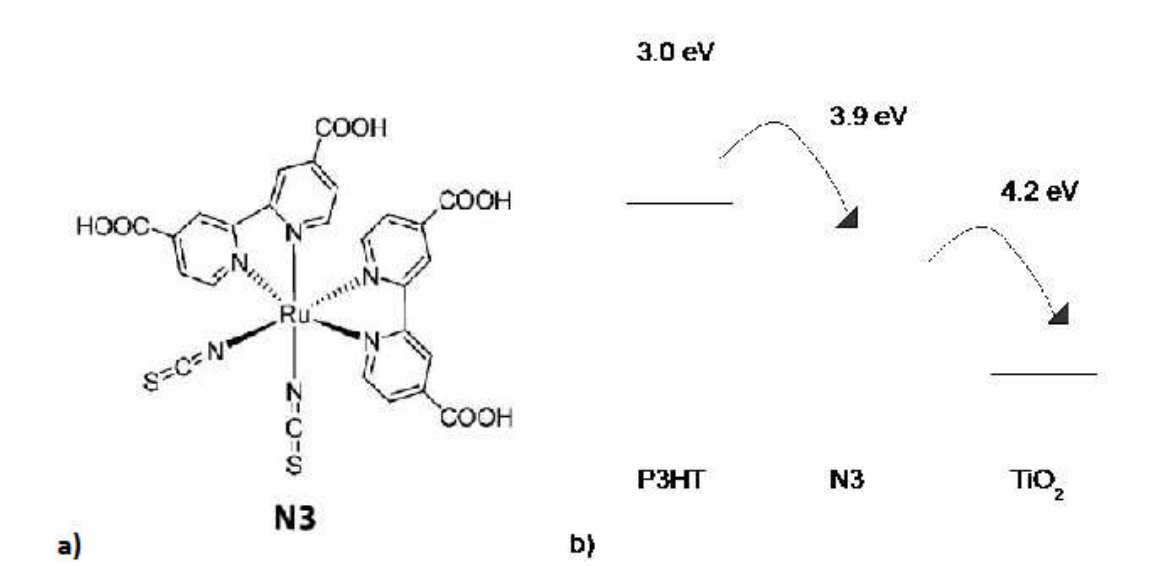

Figure 20. The chemical structure of N3 (a) and a diagram showing the energy levels an electron would pass through from P3HT to TiO2 (b)

In addition, the wetting of the polymer layer is improved. This is known to be a problem for other polymer/metal oxide systems[51] and for P3HT:TiO_2 systems[46]. In particular it appears that the alkyl side chains of P3HT do not match with the hydrophilic TiO_2[52]. The carboxylic acid groups surrounding the N3 molecule help with the wetting of the alkyl chains on the titanium dioxide.

The N3 was dissolved in ethanol at a concentration of 0.1mM. Titanium dioxide covered substrates were soaked in an N3 solution for two hours. After this, the substrates were rinsed thoroughly in ethanol then dried in nitrogen. A small colour change in the titanium dioxide was observed.

Surface quenching experiments were performed as described above with a reference sample of fused silica and a quenching sample of N3 soaked titanium dioxide. Results are shown in Figure 21.

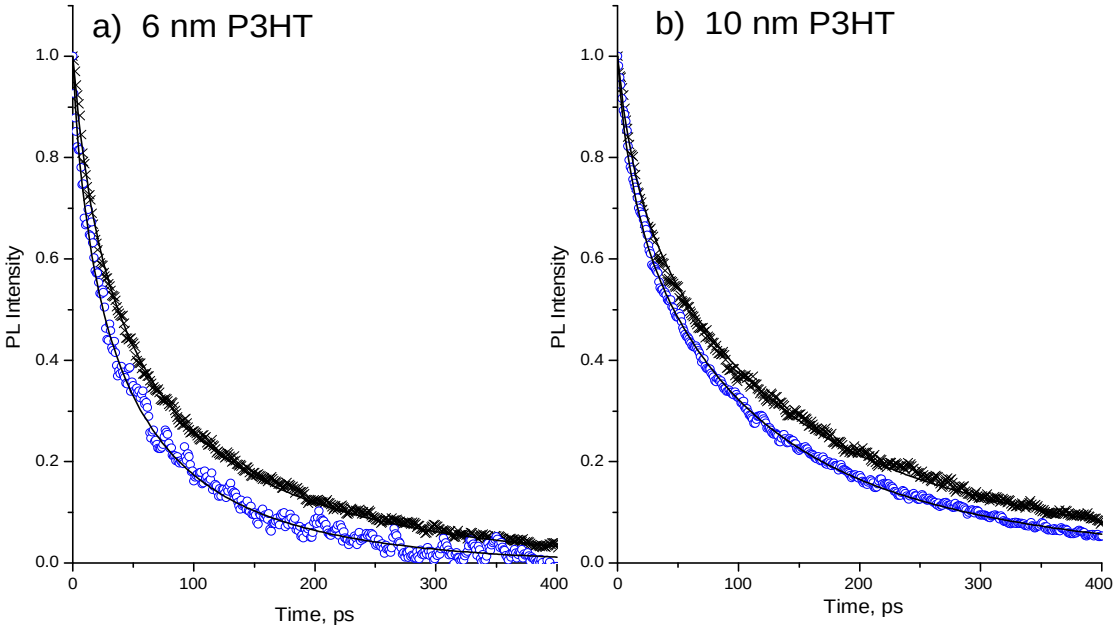

Figure 21. The PL decay of P3HT films of thickness a) 6 nm and b) 10 nm on fused silica (crosses) and N3 treated titanium dioxide (circles). The PL decay of P3HT on N3 treated TiO2 is faster in both cases, indicating that PL quenching is occurring. The solid lines show fits using the diffusion model. The value of the diffusion coefficient fitted was 0.02 nm^2ps^{-1} for a) and 0.03 nm^2ps^{-1} for b)

As the PL decay of P3HT on N3 soaked TiO_2 is slightly faster than on fused silica, it can be assumed that electron transfer from the P3HT to the TiO_2 has occurred. Excitons have therefore been separated at the titanium dioxide /P3HT interface. The diffusion of excitons was modelled, and a diffusion coefficient of 0.02 nm^2ps^{-1} was found for the 6 nm thick P3HT film. For the 10 nm thick film a diffusion coefficient of 0.03 nm^2ps^{-1} was found.

The diffusion coefficients measured were approximately a factor of ten smaller than the generally accepted value. The most likely reason for this small value is that not all excitons which reach the interface are being quenched. These results demonstrate that while N3 soaked titanium dioxide produces better quenching than titanium dioxide that is prepared on its own, the quenching is still much less than observed by Shaw et al[12].

Chapter 6

Surface Quenching Measurements Using Other Quenchers

Though titanium dioxide is the most commonly used metal oxide in surface quenching measurements, it is not the only substance which is suitable for this purpose. Any substance can quench P3HT, providing that the energy levels are appropriately matched such that an electron (or hole) can pass to the quencher. For the experiment to be successful, it is preferable if the quencher is transparent in the visible region and creates clearly defined interfaces. These two factors mean it is possible to ensure excitons are created evenly throughout the polymer film, and that quenching occurs only at defined points. These two factors are important as boundary conditions in the diffusion modelling, and significantly aid the ease with which knowledge of diffusion lengths can be taken from surface quenching experiments.

Substances which meet these conditions include zinc oxide, which is often used to make zinc oxide/ P3HT solar cells. In addition, various small molecules, such as NTCDA can be used.

6.1 Zinc oxide

Zinc oxide is a wide band gap semiconductor which is transparent in the visible range. It is an excellent electron conductor, and for this reason zinc oxide is increasingly used as an electrode in electronics applications[53]. Due to its transparency and electron conduction zinc oxide is a good candidate for the quencher in surface quenching experiments. It is possible to make ZnO:P3HT solar cells, so the principle of electron transfer from P3HT to zinc oxide has already been demonstrated[54].

Given the proven conducting properties of zinc oxide, it is a reasonable candidate for surface quenching experiments. Samples of zinc oxide from three collaborators were sourced and tested for surface quenching.

Methods of preparing zinc oxide are similar to those used for titanium dioxide. Two samples were prepared using spray pyrolysis. These were sourced from Dr Thomas Anthopoulos of Imperial College and Dr Henry Snaith of Oxford University. In addition, a sample prepared on sapphire by pulsed laser deposition was sourced from Dr Dave Rogers of Nanovation Inc.

These three samples were investigated to look for surface quenching properties.

6.1.1 Sample Preparation

Surface quenching experiments were conducted in the manner described in detail in Chapter 2 and Chapter 5. The zinc oxide samples were cleaned with acetone and IPA before use. All zinc oxide samples were found to conduct when a multimeter was used to measure resistance. The reference samples on which no quenching is expected to occur were prepared on fused silica discs. The P3HT films were prepared on top of the zinc oxide and reference substrates under identical conditions, and thickness was verified using the absorbance spectrometer.

6.1.2 Results

Results are shown below and overleaf for all three samples of zinc oxide. The reference PL decay of P3HT is shown by black crosses in all cases. The PL decay of P3HT on zinc oxide is shown by blue hollow circles. The zinc oxide prepared by Nanovation is shown in Figure 22. The spray pyrolysis prepared samples are shown in Figure 23 (Imperial) and Figure 24 (Oxford).

In all three cases, it can be seen that the PL decay of P3HT is slower on the zinc oxide coated substrates. This implies that quenching has not occurred, as a faster decay would be expected if quenching had occurred. Fits to the exciton diffusion model have not been performed because of this.

A possible explanation for the slower decays is that the optical field within the polymer is altered by the high refractive index of the zinc oxide. This is a known effect with titanium dioxide[23], and is likely to be present for zinc oxide as well. If the altered optical field has caused more of the excitons to be created at the polymer/oxide interface, this could lead to reduced quenching. This explanation assumes that the polymer/vacuum interface is a quenching interface (see Chapter 7).

In addition, the performance of zinc oxide/polymer solar cells is often worse than that of titanium dioxide/polymer solar cells, with the stated reason that there is poor exciton disassociation at the zinc oxide/polymer interface.

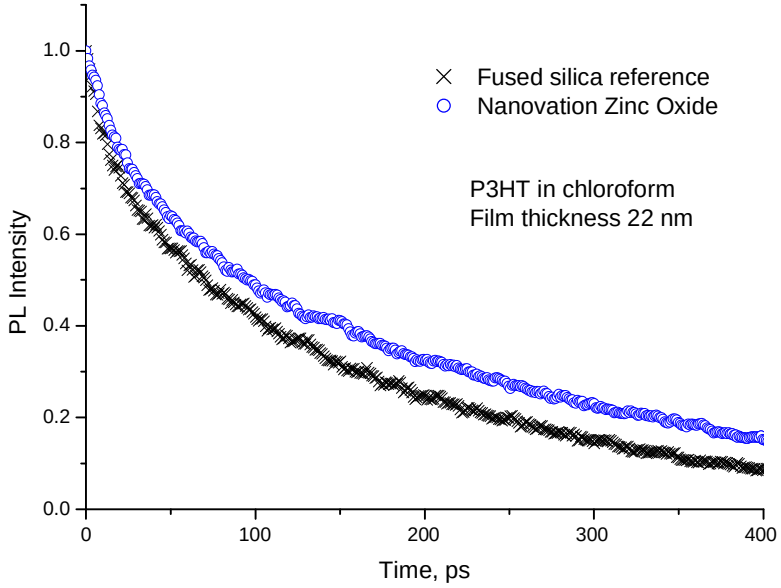

Figure 22. The PL decay of P3HT on fused silica (black crosses) and zinc oxide coated sapphire (blue circles). The Zinc Oxide was prepared by Dave Rogers of Nanovation.

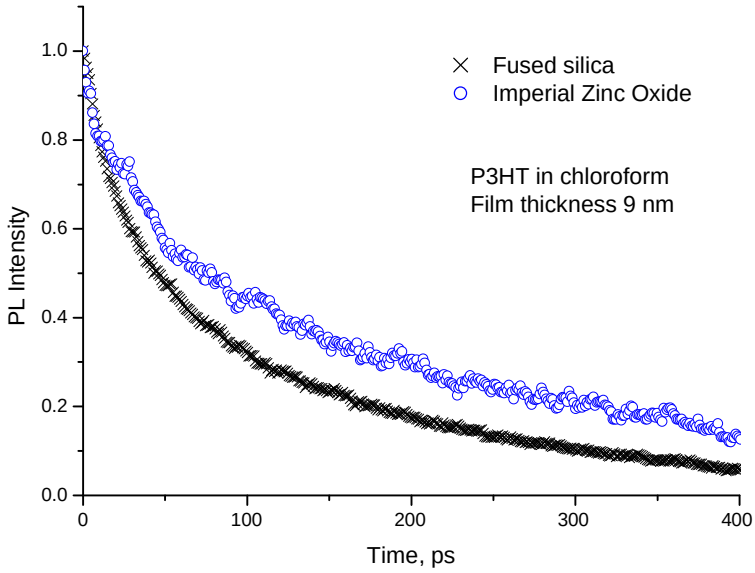

Figure 23. The PL decay of P3HT on fused silica (black crosses) and zinc oxide coated fused silica (blue circles). The Zinc Oxide was prepared by Thomas Anthopoulos of Imperial College.

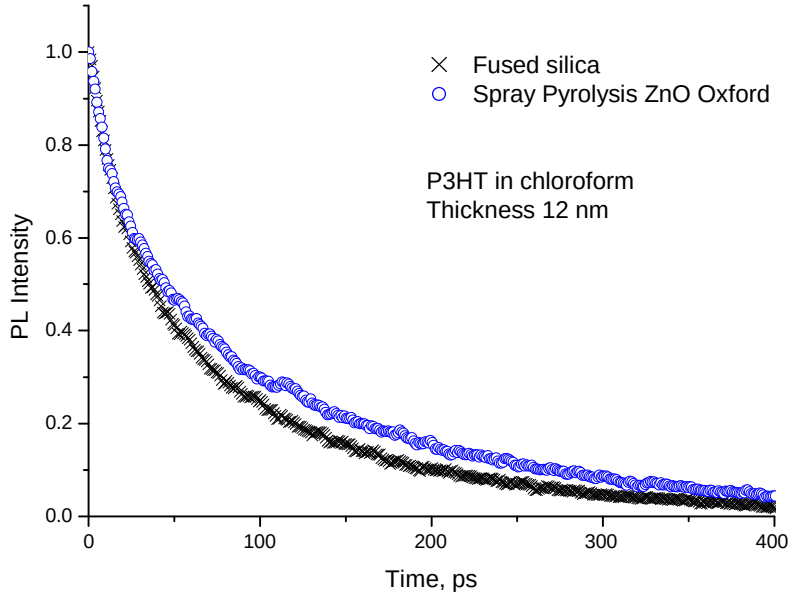

Figure 24. The PL decay of P3HT on fused silica (black crosses) and zinc oxide coated fused silica (blue circles). The Zinc Oxide was prepared with help from Henry Snaith at Oxford.

6.2 Small molecule Quenchers

Small conjugated molecules have a long history of use in organic semiconductor applications[55]. Compared to polymers, small molecule organic semiconductors generally have absorption spectra at higher frequency, due to a larger gap between the HOMO and LUMO caused by confinement of the electrons to the molecule[7]. Small molecule organic semiconductors are therefore best suited to applications in the UV and blue parts of the spectrum. They are commonly used in OLED and organic photodiode applications. Small molecules are generally prepared use evaporation techniques which are performed under vacuum.

Small molecule organic semiconductors can be used as an electron or hole acceptor, making them suitable for use in organic solar cells and as a quenching material in surface quenching experiments. The most commonly used material for this purpose is C_{60}[9,23]. Unfortunately, a problem with this material when used with P3HT in a surface quenching context is that interdiffusion of the C60 into the P3HT can occur, meaning the experiment is actually a volume quenching experiment not surface quenching. Another problem is that Förster transfer is possible due to the overlap in the absorption and emission spectra. This can increase the area over which quenching is possible, invalidating the boundary conditions for a surface quenching experiment.

Another small molecule which is suitable for surface quenching experiments in 1,4,5,8-napthalene-tetracarboxylic-dianhydride (NTCDA). NTCDA has a LUMO of 4 eV and a HOMO of 7.97 eV. It is therefore possible for electrons to transfer from P3HT to NTCDA, causing quenching of the excitons.

NTCDA is not suitable for deposition under the polymer as it is slightly soluble in chloroform and chlorobenzene, the solvents used for P3HT. If a polymer is spin cast on top of a film of NTCDA the solvent will disturb the NTCDA, allowing interdiffusion of the quencher to occur. This invalidates the boundary condition of a smooth quenching surface. This problem can be avoided by evaporating the NTCDA on top of the polymer.

As it is possible that quenching is occurring at the polymer/vacuum interface, a reference sample must also be capped with a small molecule, but this molecule must block the excitons to create an exciton reflecting interface. The molecule used for this is bathocuproine (BCP), which has a LUMO of 3.5 eV and a HOMO of 7 eV. Neither electrons nor holes can transfer from P3HT to the BCP due to the exciton binding energy being greater than the difference between the LUMO levels.

6.2.1 Sample Preparation

The P3HT was prepared by spin-coating from chloroform solutions. Concentrations from 1 mg/ml to 4 mg/ml were used to create different thicknesses of polymer film. A 20 nm layer of either BCP or NTCDA was deposited on top of the polymer films by evaporation.

6.2.2 Results and Discussion

The PL decays were measured using the streak camera and laser described in Chapter 2. PL decays are shown below in Figure 25 for P3HT films ranging in thickness from 5 nm to 28 nm. The BCP topped reference decays are shown by black circles, and the NTCDA topped quenching decays are shown by green squares. A large difference can be seen between the PL decays, with the NTCDA topped quenching decay significantly faster than the reference decay for all samples. This demonstrates that quenching of excitons has occurred.

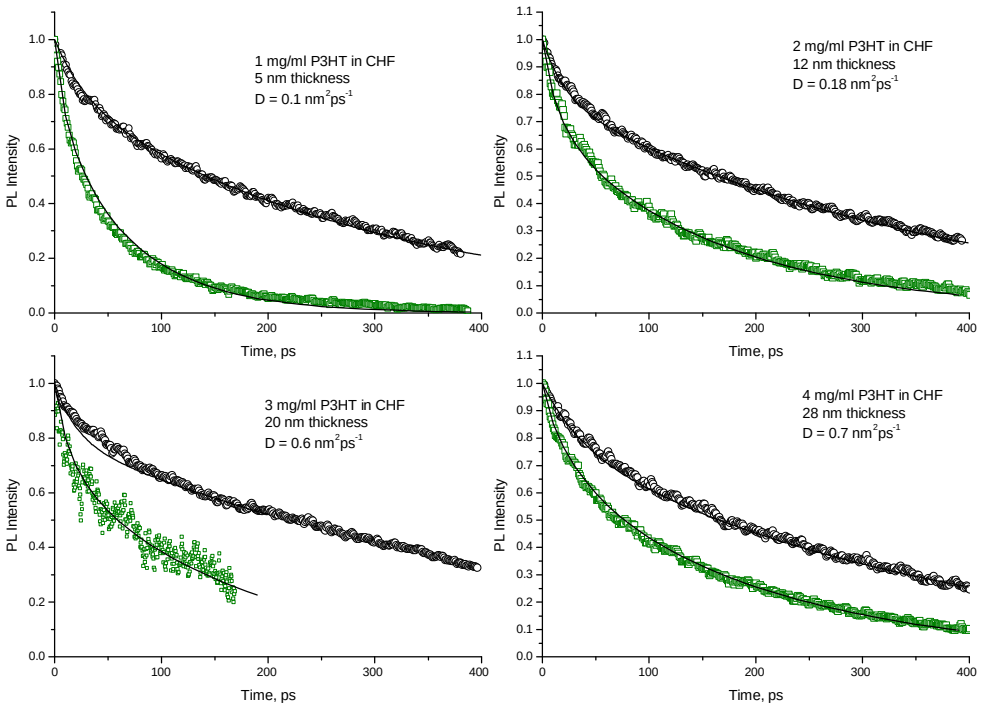

Figure 25. The PL decay of P3HT films of varying thickness capped with 20 nm of NTCDA (green circles) or 20 nm of BCP (black squares). Fits to the data for exciton diffusion are also shown (black lines), with the calculated diffusion coefficients annotated.

The fitted decays using the exciton diffusion model described earlier are also shown with black lines. The diffusion coefficients found using the model are shown in Figure 26. There are two additional data points at thicknesses 4 nm and 26 nm for which the PL decays are not shown here. A clear trend can be seen in the diffusion coefficients, with larger diffusion coefficients corresponding to thicker films.

The increase in the diffusion coefficient with the thickness of the polymer film implies that there is increased quenching present in the thicker films. The most plausible cause of this is an increase in the quenching interface available caused by diffusion of the NTCDA into the polymer. This would increase exciton quenching leading to an increase in the apparent diffusion coefficient. It is known that when aluminium is evaporated onto polymer layers as the electrode is solar cell applications the aluminium can penetrate into the polymer to a depth of 40 nm. It is believed that C60/PCBM can also diffuse into polymer layers[9]. It is likely that a similar effect can occur with NTCDA.

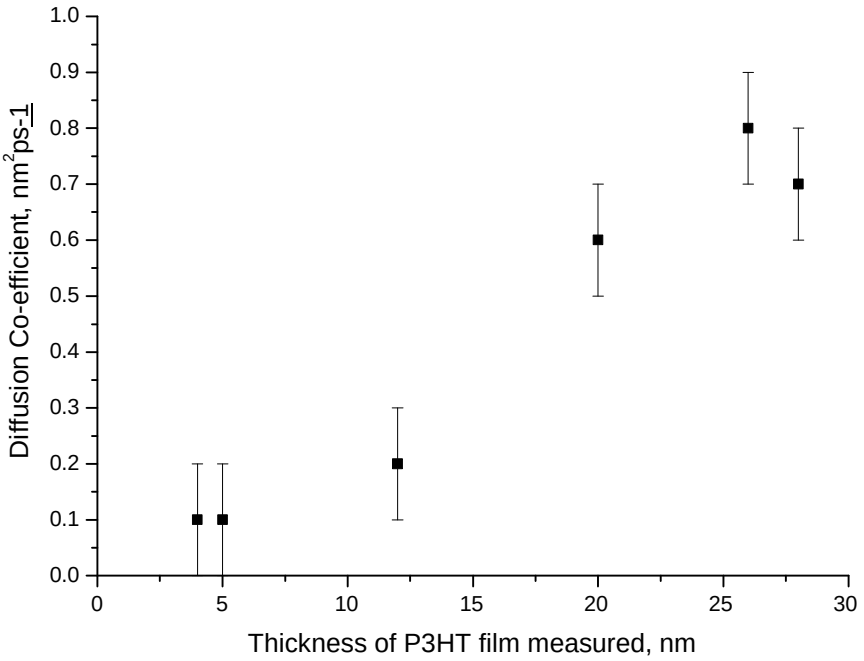

Figure 26. The diffusion coefficients found by comparing NTCDA capped and BCP capped P3HT films.

Chapter 7

Thickness Dependence of the Photoluminescence Decay Lifetime in Conjugated Polymers

7.1 Introduction

Thin films of semiconducting polymers are of increasing importance to a burgeoning organic electronics industry. It is therefore important to understand the properties of these films and how they relate to the structure of the materials and the deposition process.

One effect known to occur in thin organic films is a decrease in the photoluminescence lifetime of the polymer as the thickness of the film decreases. This could be due to an increase in the radiative decay rate, or due to an increase in the non-radiative decay rate. An example of this is shown in Figure 27, which shows the PL decays of different thicknesses of P3HT film. It can be seen that the 5 nm film has a faster decay than the 15 nm film, which is in turn faster than the 40 nm film. There is a clear relationship between the film thickness and the PL decay lifetime.

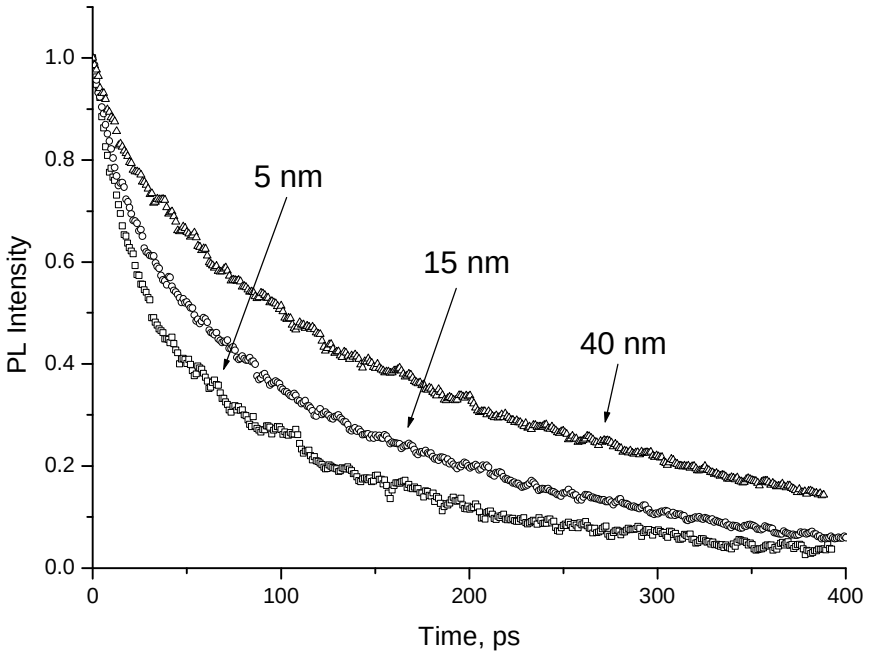

Figure 27. The PL decay of P3HT films of varying thickness. The thinnest film, at 5 nm, has the fastest PL decay. The thickest film, at 40 nm has the slowest decay.

This phenomenon has been discussed in depth by Shaw in his PhD thesis[19]. Results are presented which demonstrate the universality of the effect in polymers such as PFO, P3HT and MEH-PPV. Quenching induced by the substrate is considered as possible cause, and tested using fused silica substrates and surface passivators to reduce the possibility of quenching. This technique has had great effect in organic transistors at increasing the charge mobility near electrodes[56]. No difference was observed between reference films and those where the substrate had been passivated by Shaw, indicating that quenching by the substrate is unlikely to be the cause of the observed thickness dependence.

The effect of oxygen exposure during the film preparation stage was also investigated by Shaw. Oxygen is known to quench emission from organic semiconductors[47,57]. Films spun in an oxygen free glove box were compared with those spun in air. The film spun in air had a faster PL decay, implying that oxygen captured in the film during spin coating was quenching luminescence. However, the PL decays of the films spun in the glove box still showed thickness dependence, indicating that quenching caused by oxygen trapped in the films is not the sole cause.

Shaw concludes that the explanation for the thickness dependence is a change in the morphology of the films. This was supported by other literature[58] looking at the glass transition of polymers in thin film, which also demonstrates a thickness dependence.

Other researchers have found that the radiative decay rate may be changing when film thickness is decreased. Kim et al[59] studied F8BT films of thicknesses from 110 nm to 30 nm, finding a change in the PL lifetime from 1.95 ns to 2.70 ns. The PLQY remained constant, indicating that the radiative decay time had increased. This cause for this is believed to be a change in the distribution and population of emissive sites during film formation. However, it can be difficult to measure the PLQY of poorly emissive polymers such as P3HT so this approach has limitations.

In a different polymer system, Ribierre et al[60] studied two bisfluorene dendrimers and noted thickness dependence for both dendrimers, to different extents. This was attributed to different side chains on the dendrimers, implying intermolecular interactions are causing the change in PL lifetime. A study of the photoluminescence quantum yield of films of different thicknesses revealed the PLQY also decreased with thickness, implying that an increase in the non-radiative decay rate had occurred.

An increase in the non-radiative decay rate could be caused by an internal factor such as defects, or by external factors such as quenching by an external source. Mikhnenko et al[61] believe this to be the case in their study. They examine the PL decay of MDMO-PPV in a study of the temperature dependence of exciton diffusion. Thickness dependence is attributed to quenching at the free surface, with perfect quenching assumed in the model used. This approach will be considered in greater detail in the following section, with capping layers used to investigate the possibility that quenching may be occurring at the polymer/vacuum interface.

7.2 Investigation of Quenching at the Free Surface of the Polymer

During measurement of the PL decay the sample is stored in a chamber which is kept under vacuum. It was noted that when the pressure in the vacuum chamber was lower the PL lifetime of the sample was longer. As no vacuum is perfect, it is possible that residual oxygen present in the chamber could be causing quenching of the PL.

This hypothesis can be tested using capping layers to prevent the contact of oxygen with the polymer's free surface. The capping layers used were glass slides held in place with an epoxy or an exciton blocking layer as discussed in Chapter 6.

7.2.1 Sample Preparation

The P3HT used in these experiments is described in Chapter 2. The solvent used was chloroform, and solutions were made between 1 mg/ml and 3 mg/ml. Films were prepared on fused silica substrates. Spin-coating was performed inside a glove box to minimise oxygen within the film, but films were than transferred in air to the sample chamber. A vacuum was applied within the vacuum chamber, with the pressure kept at 1×10^{-4} mbar throughout all experiments. The PL decays were measured using the femtosecond time-resolved set-up described in Chapter 2.

7.2.2 Capping the Polymer/Vacuum Interface with Epoxy and Glass

After manufacture, organic semiconductor devices are often encapsulated to prevent water and oxygen entering the device. This prolongs the lifetime of the devices, allowing greater usage periods at higher performance levels. The most commonly used capping method is a small piece of glass held in position with a UV-curable epoxy.

Capping of prepared samples was performed in the glove box, with a 5 min curing period used. A schematic is shown in Figure 28. The epoxy was used as supplied and a small piece of glass was used to cover the epoxy. The epoxy covered the whole of the polymer area. A reference sample was also prepared with no capping performed.

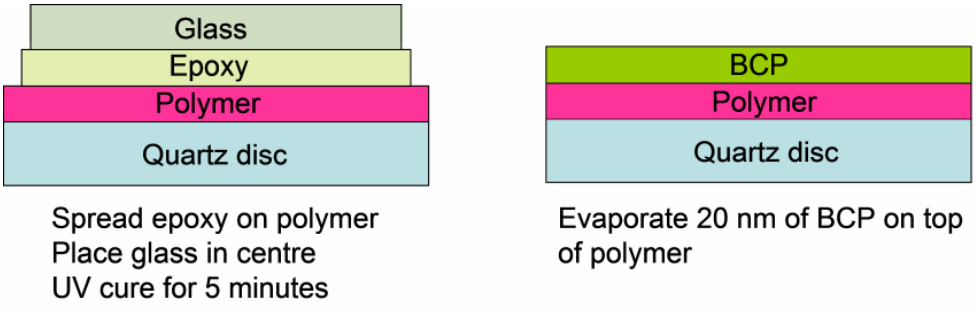

Figure 28. The different capping structures used.

The capped and reference samples were prepared in matched pairs with different P3HT film thicknesses of 5, 14 and 21 nm. The PL decay of the three capped samples and three reference samples is shown below in Figure 29. Looking at the uncapped samples, thickness dependence can again be seen, with the 5 nm sample having the fastest decay and the 21 nm sample the slowest decay. Comparing the uncapped and capped samples a large difference can be seen, with the capped samples having much slower decays than the uncapped samples. This is a clear indicator that a quenching mechanism is present in the uncapped samples. The capped samples show slight thickness dependence, with the 5 nm sample having the fastest decay and the 21 nm sample the slowest. However, it can be seen that the thickness dependence is reduced compared to the uncapped samples.

The continued presence of thickness dependence in the capped samples is attributed to oxygen trapped within the epoxy layer. Although capping was performed inside a glovebox, the equipment used was not at full functionality at the time of the experiment. Additionally it could be that the epoxy does not create a perfect seal.

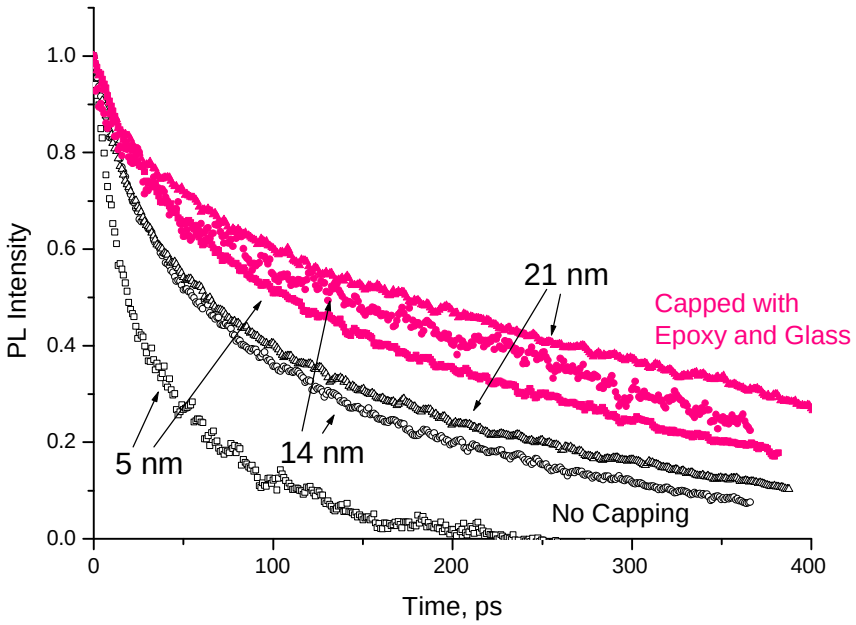

Figure 29. The PL decay of P3HT films of different thicknesses on fused silica substrates. Three of the samples were capped with epoxy (pink filled symbols) and three were uncapped (black unfilled symbols). The thicknesses were 5 nm (circles), 14 nm (squares) and 21 nm (triangles).

The data presented in Figure 29 clearly shows that the uncapped samples have much faster decays than the capped samples. A potential explanation for this could be a difference in the polymer crystallinity of the two samples. Absorbance spectra (not shown) confirmed that the polymer was in the same state in both samples, ruling out this option. In addition a small difference in crystallinity is unlikely to have such a large effect on the decay.

Another explanation is that the polymer/vacuum interface in the uncapped samples is a quenching interface. Using the surface quenching model discussed in Chapter 5 this can be investigated. Figure 30 below shows the same data as presented in Figure 29 with fits generated by the surface quenching model discussed earlier in Chapter 5. Here the epoxy capped sample is considered the reference sample and the uncapped sample is considered the quenching sample.

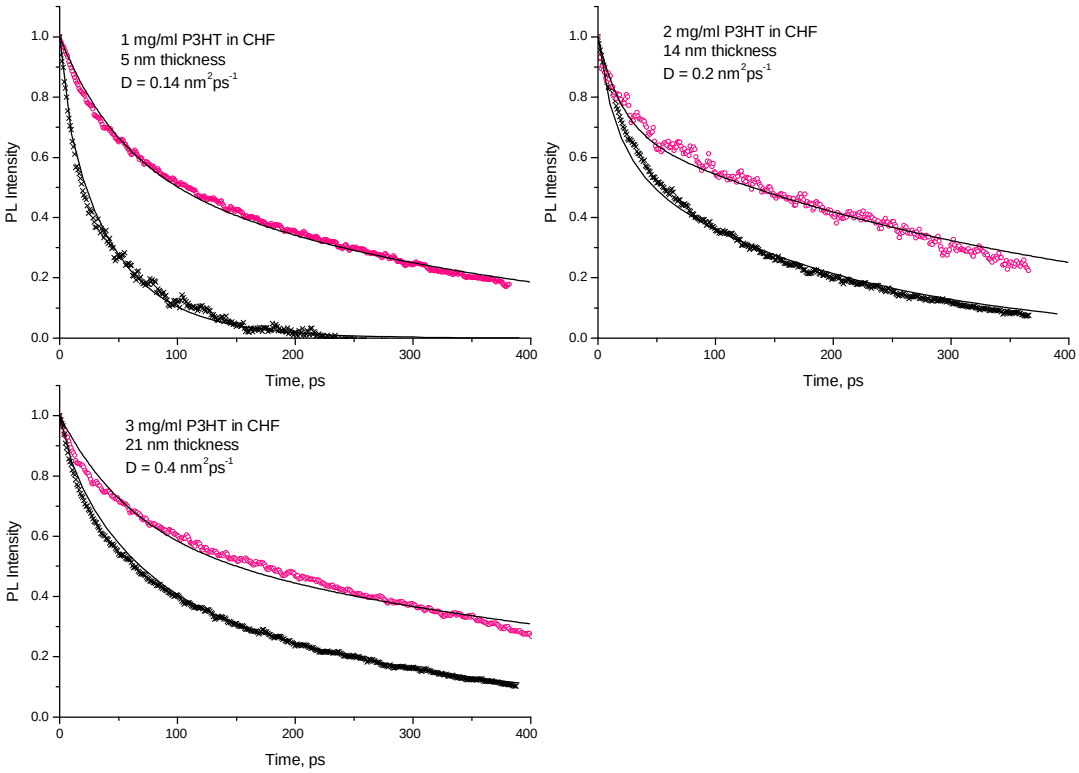

Figure 30 The PL decay of epoxy capped (pink circles) and uncapped (black crosses) P3HT samples. Fits generated using the surface quenching model are shown as black lines.

From Figure 30 it can be seen that the surface quenching model provides good fits to the experimental data. However, the diffusion coefficient calculated varies between samples. This will be discussed in more detail in Section 7.2.4.

7.2.3 Capping the Polymer/Vacuum Interface with an Exciton Blocking Layer

As discussed in Chapter 6, exciton blocking layers can be used to prevent the passage of excitons into an organic layer. Bathocuproine (BCP) is a small molecule which is deposited by evaporation under vacuum. It is often used as an exciton blocking layer in OLEDS and photodiodes.

Figure 31 shows the PL decay of different thicknesses of P3HT film capped with BCP or with no capping. Again a large difference can be seen between the PL decay of capped and uncapped samples, with the uncapped samples decaying much faster. Looking just at the uncapped samples, thickness dependence can again be seen, with the PL decay of the 5 nm film significantly faster than the PL decay of the 40 nm film. Interestingly the thickness dependence is not observed with the capped films. The PL decays of the capped films were all very close together.

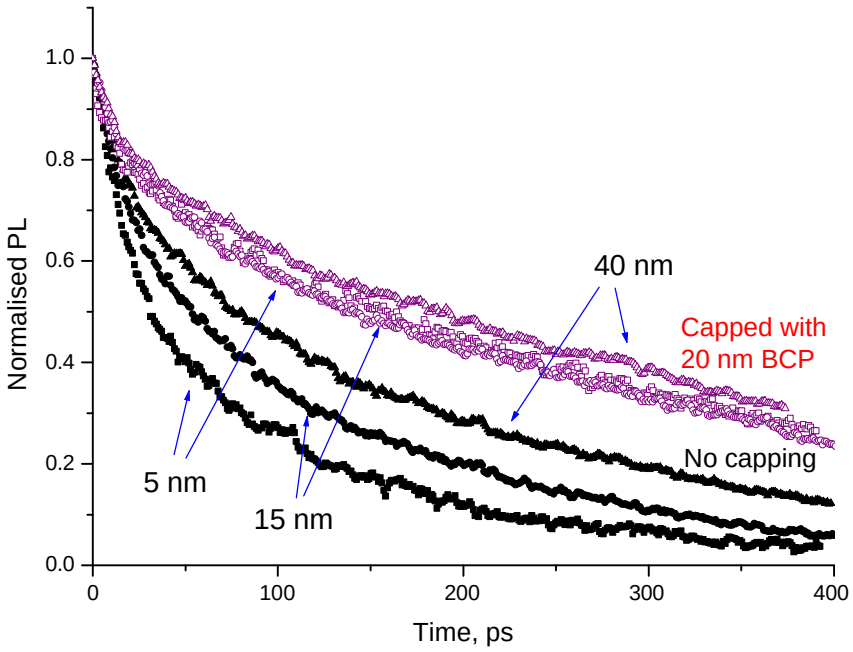

Figure 31 The PL decay of P3HT of varying thickness when capped with BCP (purple unfilled symbols) and uncapped (black filled symbols). The thicknesses of the P3HT films are 5 nm (squares), 15 nm (circles) and 40 nm (triangles).

The surface quenching model discussed in Chapter 5 was again used to fit the data. The fits are shown in Figure 32, which presents the same data as Figure 31. The BCP capped sample is the unquenched sample in the modelling, with the uncapped sample as the quenched sample. Quenching is assumed to occur at the polymer/vacuum interface. The fits prepared using the model are good, indicating that surface quenching is a reasonable explanation. Again a variation in the diffusion coefficient can be seen, which will be discussed in Section 7.2.4.

The fits to the BCP capped samples were created from a bi-exponential decay. This is different to the fit used for uncapped samples and glass capped samples, which require a tri-exponential decay for fitting. This addition of an extra component may suggest that an additional, quenching mechanism is occurring in the uncapped and glass capped samples[59].

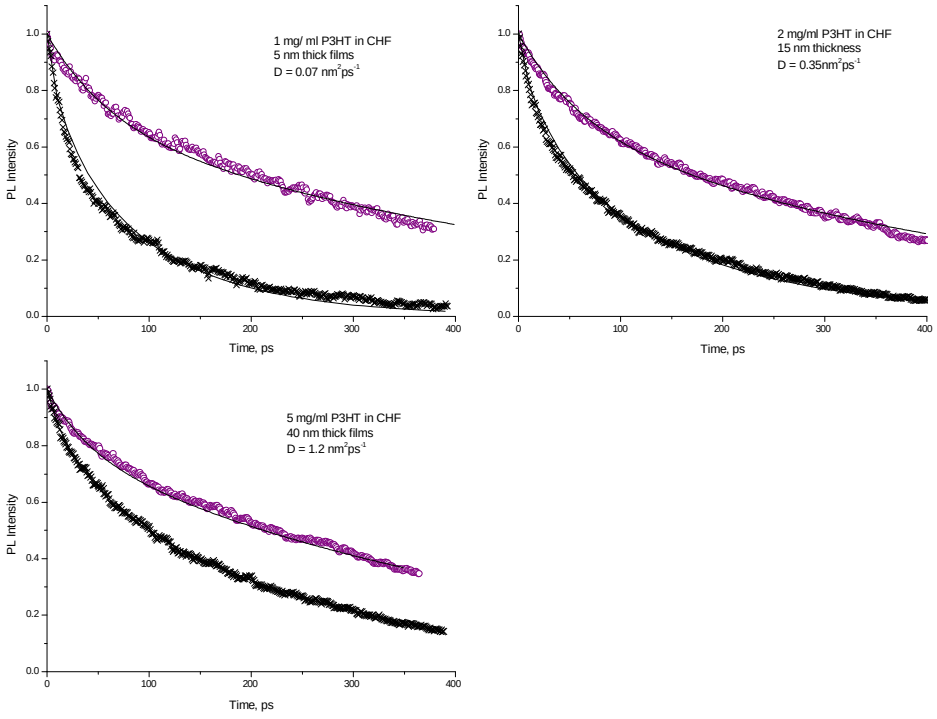

Figure 32. The PL decay of BCP capped (purple circles) and uncapped (black crosses) P3HT samples. Fits generated using the surface quenching model are shown as black lines.

7.2.4 Comparing Capping Methods

The diffusion coefficients calculated from the fits are summarised below in Figure 33. The diffusion coefficient gives a measure of the amount of quenching occurring at the quenching interface. The model assumes a perfect quencher with a smooth interface.

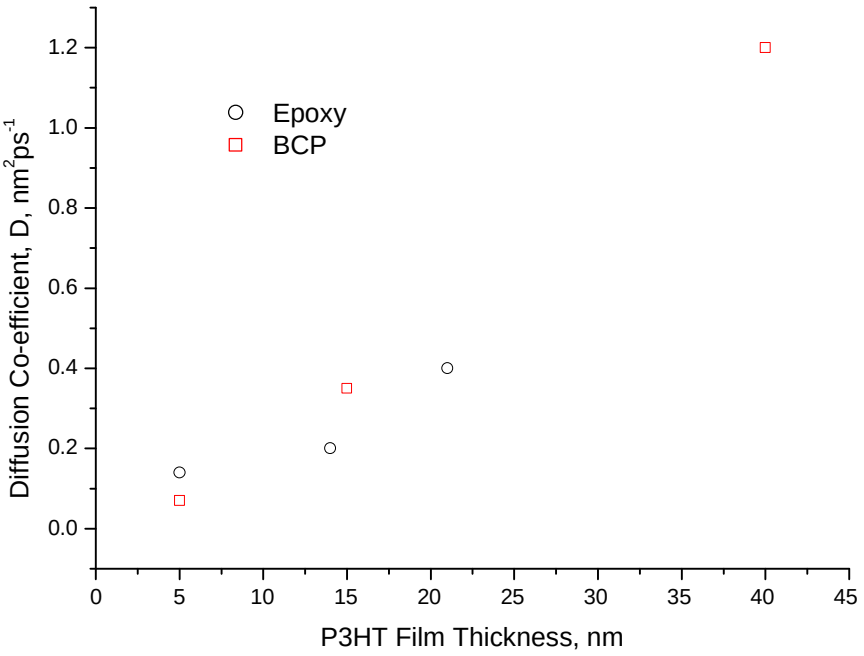

Figure 33. The diffusion coefficients found by modelling the polymer/vacuum interface as a perfect quencher. The reference sample for comparison was capped with either glass and epoxy (circles) or BCP (squares).

Figure 33 shows a strong correlation between the diffusion coefficient and the thickness of the P3HT layer. As discussed in Chapter 6, the most likely reason for an increase in the exciton diffusion length as the polymer film thickness increases is inter-diffusion of the quencher into the polymer.

It is proposed that the quenching observed here is caused by oxygen present within the chamber. It is known that gases can penetrate into polymer layers and induce quenching within[62]. Oxygen is a strong quencher of photoluminescence.

This is supported by the observation of decreasing PL decay time when the sample is under a high vacuum (~10^{-6} mbar).

Oxygen quenching is also proposed as an explanation of the difference between capping with epoxy and glass versus BCP. The epoxy was applied in a glovebox which may have been contaminated with oxygen at the time. Oxygen could have become trapped in the epoxy layer, causing quenching of the sample when excited.

Chapter 8

Conclusion

Organic solar cells show great potential as sources of clean energy, yet challenges remain with low efficiencies. A likely method for improving efficiency is through optimization and understanding of the exciton diffusion process within the donor material.

This work details ultrafast photophysical measurements made to measure the exciton diffusion length in a common donor material ,P3HT. The experiment consisted of preparing thin polymer samples, measuring the film thickness through ellipsometry, measuring the photoluminescence decay using a streak camera, and comparing quenched and unquenched samples using a model of diffusion dynamics.

The use of ellipsometry as a robust measurement of thin film thicknesses was confirmed. Difficulties were encountered with obtaining samples of titanium dioxide quencher which provided enough separation of excitons to allow an observable difference between samples. The cause of this was believed to be problems with the titanium dioxide/polymer interface. The use of a surface modifying dye was investigated to rectify this problem. This approach was found to improve quenching, though low values of the diffusion co-efficient were still observed.

Alternative quenchers such as zinc oxide and NTCDA were also investigated. Results with zinc oxide were inconsistent, and this was attributed to the high refractive index of zinc oxide. Optical modeling of the zinc oxide/polymer system to find the optimum thickness of zinc oxide would be a solution to this problem. The quenching caused by NTCDA was found to vary with the thickness of the polymer, which is believed to be caused by the interdiffusion of the NTCDA into the polymer. This is likely to be a problem for all small molecules which must be deposited through vacuum evaporation.

The thickness dependence of the polymer's photoluminescence decay was also investigated using two different capping techniques: a small molecule exciton blocker, and an epoxy used for encapsulating organic solar cells. The photoluminescence decay rate is found to increase as the thickness of a polymer film decreases. This effect was found to be vastly reduced by adding a capper to the polymer. This implies that the increase in the decay rate is caused by quenching at the free interface of the polymer, with the capping layers preventing this quenching from occurring. It was also found that the exciton blocking molecule was better at preventing this quenching than the epoxy, which could be considered in the design of improved epoxies.

Acknowledgements

I would like the thank Professor Ifor Samuel for giving me the opportunity to study at St Andrews, for gracefully accepting my decision to leave, and for his help in suggesting improvements to this thesis. I would like to thank Aryvdas Ruseckas for allowing me to work in his wonderful femto-lab, for his patience with my many questions and for his good humour.

I would also like to thank the members of the Polyopto group, in particular Georgios Tsiminis, Jack Levell, Gordon Hedley, Ashu Bansal and the irrepressible Calvyn Travis Howells for their help and camaraderie. Thanks also to Paul Dalgarno and Mario Giardini for wise words at crucial times. A special thank you to the vital support staff, Steve Balfour and Scott Richardson.

Thank you to my family for their support, and to Will Harris for his love and encouragement.

References

1 Jones, R A L, in *Soft Machines* (2010), pp. Soft Machines Blog.

2 Solar energy incident on Earth's surface. Calculated for an average sized 500 MW coal power station.

3 REN21, 2006.

4 NREL, Available at http://www.nrel.gov/news/press/2008/625.html, (2008).

5 Solarmer, Available at http://www.solarmer.com/newsevents.php, (2010).

6 Slyke, S. A. Van, Chen, C. H., and Tang, C. W., Organic electroluminescent devices with improved stability. *Applied Physics Letters* **69** (15), 2160 (1996).

7 Fox, Mark, *Optical Properties of Solids*. (2007).

8 M Pope, C E Swenburg, *Electronic Processes in Organic Crystals and Polymers*, 2nd ed. (1999).

9 A L Azyner, C J Tassone, S H Tolbert, B J Schwartz, Reappraising the Need for Bulk Heterojunctions in Polymer-Fullerene Photovoltaics: The Role of Carrier Transport in All-Solution-Processed P3HT/PCBM Bilayer Solar Cells. *Journal of Chemical Physics* **113**, 20050 (2009).

10 M Koppe, H-J Egelhaaf, G Dennler, M C Scharber, C J Brabec, P Schilinsky and C N Hoth, Near IR Sensitisation of Organic Bulk Heterojunction Solar Cells: Towards Optimisation of the Spectral Response of Organic Solar Cells. *Advanced Materials* (2009).

11 BAVEL, VAN et al., *Relation between Photoactive Layer Thickness, 3D Morphology, and Device Performance in P3HT/PCBM Bulk-Heterojunction Solar Cells*. (American Chemical Society, Washington, DC, ETATS-UNIS, 2009).

12 Shaw, P. E., Ruseckas, A., and Samuel, I. D. W., Exciton diffusion measurements in poly(3-hexylthiophene). *Advanced Materials* **20** (18), 3516 (2008).

13 Choulis. *Applied Physics Letters* **3890** (2004).

14 Pettersson, Leif A. A., Roman, Lucimara S., and Inganas, Olle, Modeling photocurrent action spectra of photovoltaic devices based on organic thin films. *Journal of Applied Physics* **86** (1), 487 (1999).

15 Stubinger, T. and Brutting, W., Exciton diffusion and optical interference in organic donor-acceptor photovoltaic cells. *Journal of Applied Physics* **90** (7), 3632 (2001).

16 C Muller, T A M Ferenczi, M Campoy-Quiles, J M Frost, D D C Bradley, P Smith, N Stingelin-Stutzmann and J Nelson, Binary Organic Photovoltaic Blends: A Simple Rationale for Optimum Compositions. *Advanced Materials* **20**, 3510 (2008).

17 Jones, R A L, *Soft Condensed Matter*. (2002).

18 Nelson, J., Organic photovoltaic films. *Current Opinion in Solid State & Materials Science* **6** (1), 87 (2002).

19 Shaw, Paul E, University of St Andrews, 2009.

20 A Ruseckas, P Shaw, I D W Samuel, Probing the nanoscale phase separation in binary photovoltaic blends of poly(3-hexylthiophene) and methanofullerene by energy transfer. *Dalton Transactions*, 10040 (2009).

21 Greenham, N. C. et al., Measurement of absolute photoluminescence quantum efficiencies in conjugated polymers. *Chemical Physics Letters* **241** (1-2), 89 (1995).

[22] Kawamura, Y., Yanagida, S., and Forrest, S. R., Energy transfer in polymer electrophosphorescent light emitting devices with single and multiple doped luminescent layers. *Journal of Applied Physics* **92** (1), 87 (2002).

[23] S R Scully, M D McGehee, Effects of Optical Interference and Energy Transfer on Exciton Diffusion Length Measurements in Organic Semiconductors. *Journal of Applied Physics* **100** (034907) (2006).

[24] Hennebicq, E. et al., Exciton migration in rigid-rod conjugated polymers: An improved Forster model. *J. Am. Chem. Soc.* **127** (13), 4744 (2005).

[25] Daniel, C. et al., The effects of supramolecular assembly on exciton decay rates in organic semiconductors. *Journal of Chemical Physics* **123** (8), 7 (2005).

[26] Virkar, A. A., Mannsfeld, S., Bao, Z. A., and Stingelin, N., Organic Semiconductor Growth and Morphology Considerations for Organic Thin-Film Transistors. *Advanced Materials* **22** (34), 3857.

[27] R R Lunt, J B Benziger, S R Forrest, Relationship between crystalline order and exciton diffusion length in molecular organic seminconductors. *Advanced Materials* **22**, 1233 (2010).

[28] Burlakov, V. M. et al., Discrete hopping model of exciton transport in disordered media. *Physical Review B* **72** (7), 075206 (2005).

[29] Amarasinghe, Vithanage Chiranthika Dimali, University of St Andrews, 2008.

[30] Ramsdale, C. M. and Greenham, N. C., The optical constants of emitter and electrode materials in polymer light-emitting diodes. *Journal of Physics D: Applied Physics* **36** (4), L29 (2003).

[31] Maria, Losurdo, Giovanni, Bruno, and Eugene, A. Irene, Anisotropy of optical properties of conjugated polymer thin films by spectroscopic ellipsometry. *Journal of Applied Physics* **94** (8), 4923 (2003).

[32] Zhang, Yong, Wang, Chengwei, Rothberg, Lewis, and Ng, Man-Kit, Surface-initiated growth of conjugated polymers for functionalization of electronically active nanoporous networks: synthesis, structure and optical properties. *Journal of Materials Chemistry* **16** (37), 3721 (2006).

[33] McBranch, D.; Campbell, I. H.; Smith, D. L.; Ferraris, J. P, Optical determination of chain orientation in electroluminescent polymer films. *Applied Physics Letters* **66** (10), 1175 (1995).

[34] Campoy-Quiles, M., Etchegoin, P. G., and Bradley, D. D. C., Exploring the potential of ellipsometry for the characterisation of electronic, optical, morphologic and thermodynamic properties of polyfluorene thin films. *Synthetic Metals* **155** (2), 279 (2005).

[35] Losurdo, M. et al., Spectroscopic ellipsometry for characterization of organic semiconductor polymeric thin films. *Synthetic Metals* **138** (1-2), 49 (2003).

[36] Wong, Wai-Yeung et al., Metallated conjugated polymers as a new avenue towards high-efficiency polymer solar cells. *Nat Mater* **6** (7), 521 (2007).

[37] Tompkins, Harland ed., *Handbook of Ellipsometry*. (2005).

[38] C M Ramsdale, N C Greenham, Ellipsometric Determination of Anisotropic Optical Constants in Electroluminescent Conjugated Polymers. *Advanced Materials* **14** (3) (2002).

[39] McGehee, M. D. and Heeger, A. J., Semiconducting (Conjugated) Polymers as Materials for Solid-State Lasers. *Advanced Materials* **12** (22), 1655 (2000).

[40] Olivier, P. M. Gaudin, Ifor, D. W. Samuel, Samia, Amriou, and Paul, L. Burn, Thickness dependent absorption spectra in conjugated polymers: Morphology or interference? *Applied Physics Letters* **96** (5), 053305.

[41] Shi, Y., Liu, J., and Yang, Y., Device performance and polymer morphology in polymer light emitting diodes: The control of thin film morphology and device quantum efficiency. *Journal of Applied Physics* **87** (9), 4254 (2000).

[42] X Yang, J Loos, Toward High-Performance Polymer Solar Cells: The Importance of Morphology Control. *Macromolecules* **40** (5) (2007).

[43] X Wang, D ZHang, K Braun, H-J Egelhaaf, C J Brabec, A J Meixner, HIgh Resolution Spectroscopic Mapping of the Chemical Contrast from Nanometer Domains in P3HT:PCBM Organic Blends for Solar-Cell Applications. *Advanced Functional Materials* **20**, 492 (2010).

[44] van Duren, J. K J et al., Relating the Morphology of Poly(p-phenylene vinylene)/Methanofullerene Blends to Solar-Cell Performance. *Advanced Functional Materials* **14** (5), 425 (2004).

[45] Gregg, Brian A., Sprague, Julian, and Peterson, Mark W., Long-Range Singlet Energy Transfer in Perylene Bis(phenethylimide) Films. *The Journal of Physical Chemistry B* **101** (27), 5362 (1997); Markov, Denis E. et al., Accurate Measurement of the Exciton Diffusion Length in a Conjugated Polymer Using a Heterostructure with a Side-Chain Cross-Linked Fullerene Layer. *The Journal of Physical Chemistry A* **109** (24), 5266 (2005).

[46] C Goh, S R Scully, M C McGehee, Effects of Molecular Interface Modification in Hybrid Organic-Inorganic Photovoltaic Cells. *Journal of Applied Physics* **101** (114503) (2007).

[47] Lüer, L. et al., Oxygen-induced quenching of photoexcited states in polythiophene films. *Organic Electronics* **5** (1-3), 83 (2004).

[48] Markov, D. E. and Blom, P. W. M., Anisotropy of exciton migration in poly(p -phenylene vinylene). *Physical Review B* **74** (8), 085206 (2006).

[49] Kroeze, Jessica E., Savenije, Tom J., Vermeulen, Martien J. W., and Warman, John M., Contactless Determination of the Photoconductivity Action Spectrum, Exciton Diffusion Length, and Charge Separation Efficiency in Polythiophene-Sensitized TiO2 Bilayers. *The Journal of Physical Chemistry B* **107** (31), 7696 (2003).

[50] Stevens, Mark A., Silva, Carlos, Russell, David M., and Friend, Richard H., Exciton dissociation mechanisms in the polymeric semiconductors poly(9,9-dioctylfluorene) and poly(9,9-dioctylfluorene-co-benzothiadiazole). *Physical Review B* **63** (16), 165213 (2001); Lewis, A. J. et al., Singlet exciton diffusion in MEH-PPV films studied by exciton-exciton annihilation. *Organic Electronics* **7** (6), 452 (2006).

[51] W J Mitchell, P L Burn, R K Thomas, G Fragneto, J P J Markham and I D W Samuel, Relating the physical structure and optical properties of conjugated polymers using neutron reflectivity in combination with photoluminescence spectroscopy. *Journal of Applied Physics* **95** (5), 2391 (2004).

[52] C Hsu, L Wang, W Su, Effect of chemical structure of interface modifier of TiO2 on photovoltaic properties of P3HT/TiO2 layered solar cells. *Journal of Colloid and Interface Science* **329**, 182 (2009).

[53] Song, M. H. et al., Optically-Pumped Lasing in Hybrid Organic-Inorganic Light-Emitting Diodes. *Advanced Functional Materials* **19** (13), 2130 (2009).

[54] Punniamoorthy Ravirajan, Ana M. Peiro, Mohammad K. Nazeeruddin, Michael Graetzel, and Donal D. C. Bradley, James R. Durrant, and Jenny Nelson,, Hybrid Polymer/Zinc Oxide Photovoltaic Devices with Vertically Oriented ZnO Nanorods and an Amphiphilic Molecular Interface Layer. *Journal of Physical Chemistry B* **110**, 7635 (2006).

[55] Powell, R. C., THERMAL AND SAMPLE-SIZE EFFECTS ON FLUORESCENCE LIFETIME AND ENERGY TRANSFER IN

TETRACENE-DOPED ANTHRACENE. *Physical Review B* **2** (6), 2090 (1970).

[56] Kline, R. J., McGehee, M. D., and Toney, M. F., Highly oriented crystals at the buried interface in polythiophene thin-film transistors. *Nat. Mater.* **5** (3), 222 (2006).

[57] Farmilo, A. and Wilkinso.F, MECHANISM OF QUENCHING OF SINGLET OXYGEN IN SOLUTION. *Photochem. Photobiol.* **18** (6), 447 (1973).

[58] C J Ellison, J M Torkelson, The distribution of glass-transition temperatures in nanoscopically confined glass formers. *Nature Materials 2*, 695 (2003); Campoy-Quiles, M., Sims, M., Etchegoin, P. G., and Bradley, D. D. C., Thickness-Dependent Thermal Transition Temperatures in Thin Conjugated Polymer Filmsâ€ *Macromolecules* **39** (22), 7673 (2006).

[59] Kim, J. S., Friend, R. H., Grizzi, I., and Burroughes, J. H., Spin-cast thin semiconducting polymer interlayer for improving device efficiency of polymer light-emitting diodes. *Applied Physics Letters* **87** (2), 3 (2005).

[60] Ribierre, J. C. et al., Thickness Dependence of the Fluorescence Lifetime in Films of Bisfluorene-Cored Dendrimers. *J. Phys. Chem. C* **112** (51), 20463 (2008).

[61] Mikhnenko, O. V. et al., Temperature dependence of exciton diffusion in conjugated polymers. *Journal of Physical Chemistry B* **112** (37), 11601 (2008).

[62] Yang, Ying, Turnbull, Graham A., and Samuel, Ifor D. W., Sensitive Explosive Vapor Detection with Polyfluorene Lasers. *Advanced Functional Materials* **20** (13), 2093.